Measurement of the branching ratio for $\eta \to \pi^0\gamma\gamma$ decay

S. Prakhov,[1] B. M. K. Nefkens,[1] C. E. Allgower,[2,*] V. Bekrenev,[3] W. J. Briscoe,[4] M. Clajus,[1] J. R. Comfort,[5] K. Craig,[5] D. Grosnick,[6] G. M. Huber,[8] D. Isenhower,[7] N. Knecht,[8] D. Koetke,[6] A. Koulbardis,[3] N. Kozlenko,[3] S. Kruglov,[3] G. Lolos,[8] I. Lopatin,[3] D. M. Manley,[9] R. Manweiler,[6] A. Marušić,[1,†] S. McDonald,[1,‡] J. Olmsted,[9,§] Z. Papandreou,[8] D. Peaslee,[10] N. Phaisangittisakul,[1] J. W. Price,[1] A. F. Ramirez,[5] M. Sadler,[7] A. Shafi,[4] H. Spinka,[2] T. D. S. Stanislaus,[6] A. Starostin,[1] H. M. Staudenmaier,[11] I. Supek,[12] and W. B. Tippens[1,¶]

(Crystal Ball Collaboration)

[1]*University of California Los Angeles, Los Angeles, California 90095-1547, USA*

[2]*Argonne National Laboratory, Argonne, Illinois 60439-4815, USA*

[3]*Petersburg Nuclear Physics Institute, Gatchina RU-188350, Russia*

[4]*The George Washington University, Washington, DC 20052-0001, USA*

[5]*Arizona State University, Tempe, Arizona 85287-1504, USA*

[6]*Valparaiso University, Valparaiso, Indiana 46383-6493, USA*

[7]*Abilene Christian University, Abilene, Texas 79699-7963, USA*

[8]*University of Regina, Saskatchewan, Canada S4S OA2*

[9]*Kent State University, Kent, Ohio 44242-0001, USA*

[10]*University of Maryland, College Park, Maryland 20742-4111, USA*

[11]*Universität Karlsruhe, Karlsruhe D-76128, Germany*

[12]*Rudjer Boskovic Institute, Zagreb 10002, Croatia*

(Received 19 October 2004; published 18 August 2005)

The branching ratio (BR) for the rare decay $\eta \to \pi^0\gamma\gamma$ was measured with the Crystal Ball multiphoton spectrometer. The result, $\mathrm{BR}(\eta \to \pi^0\gamma\gamma) = (3.5 \pm 0.7_{\mathrm{stat}} \pm 0.6_{\mathrm{syst}}) \times 10^{-4}$, is in agreement with calculations of chiral perturbation theory to third order. We have used a sample of 28 million η mesons produced at the BNL Alternating Gradient Synchrotron using the $\pi^- p \to \eta n$ reaction close to threshold. We detail the intricate extraction of the signal, which has about 1.6 thousand $\eta \to \pi^0\gamma\gamma$ events, from the overwhelming background of $\eta \to 3\pi^0$ decays and from the $\pi^- p \to \pi^0\pi^0 n$ reaction.

DOI: 10.1103/PhysRevC.72.025201 PACS number(s): 14.40.Aq, 13.20.−v, 12.39.Fe

I. INTRODUCTION

Quantum chromodynamics (QCD), the accepted theory for strong interactions based on quark and gluon degrees of freedom, is not useful at low energy where the quark and gluon coupling is large. The standard power series expansion in the coupling constant does not converge at low energy. A different approach is provided by chiral perturbation theory (χPTh); it uses a momentum expansion and has an extensive record of successful calculations of various quantities [1].

The decay mode $\eta \to \pi^0\gamma\gamma$ is forbidden in leading order, $\mathcal{O}(\mathrm{p}^2)$, because there is no direct coupling of photons to the neutral π^0 and η [2]. The second order, $\mathcal{O}(\mathrm{p}^4)$, is much suppressed because it involves G-parity violating transitions; its contribution to the partial decay width $\Gamma(\eta \to \pi^0\gamma\gamma)$ is only 0.004 eV [2]. In contrast to this is the third order term, $\mathcal{O}(\mathrm{p}^6)$, of χPTh, which is predicted to give 0.42 ± 0.20 eV [2]. This value is supported by other χPTh calculations as well as by evaluations based on vector-meson dominance (VMD) and other models [3–9]. Thus we have the unique case that the decay rate for $\eta \to \pi^0\gamma\gamma$ is a direct test of the correctness of the calculations of the third order χPTh, the first order being zero and the second being very small.

An anthology of the forty-plus-year history of calculating $\Gamma(\eta \to \pi^0\gamma\gamma)$ has been provided by the SND group [10] with many interesting, nuanced details. The most recent calculations are summarized in Table I. The value 0.42 ± 0.20 eV from Ref. [2] is a good representation of the theoretical predictions for $\Gamma(\eta \to \pi^0\gamma\gamma)$.

The experimental history is given in the same anthology [10]. Until 1980, there were 13 experiments with contradictory and unconvincing results because of huge neutral backgrounds coming from $\eta \to 3\pi^0$ and other processes. In 1982, the first major high-energy detector used for η-decay studies, GAMS-2000, yielded $\mathrm{BR}(\eta \to \pi^0\gamma\gamma) = (9.5 \pm 2.3) \times 10^{-4}$ [11]. The data were later reanalyzed, and a new result for the BR of $(7.1 \pm 1.4) \times 10^{-4}$ was reported in 1984 [12], based on a sample of 40 events. It implies that $\Gamma(\eta \to \pi^0\gamma\gamma) = 0.84 \pm 0.17$ eV. This width is double the χPTh calculation of 0.42 ± 0.20 eV [2] and of most other predictions (see Refs. [3–9]). The recent work of the SND collaboration at VEPP-2M gave a 90% CL upper limit on the $\mathrm{BR}(\eta \to \pi^0\gamma\gamma)$ of 8.4×10^{-4} [10]. Note that if the GAMS-2000 result were

*Present address: Midwest Proton Radiotherapy Institute, 2425 Milo B. Sampson Ln., Bloomington, IN 47408.

†Present address: Collider-Accelerator Dept., Brookhaven National Laboratory, Upton, NY 11973, USA.

‡Present address: TRIUMF, 4004 Wesbrook Mall, Vanccouver, B.C., Canada V6T 2A3.

§Present address: Physics and Computer Planning, 810 Ingraham Pl., Charlotte, NC 28270.

¶Present address: Nuclear Physics Div., Dept. of Energy, 19901 Germantown Road, Germantown, MD 20874-1290, USA.

TABLE I. Theoretical calculations for the $\eta \to \pi^0\gamma\gamma$ decay rate. ENJL—extended Nambu-Jona-Lasinio model; VMD—vector-meson-dominance model.

Theory	$\Gamma(\eta \to \pi^0\gamma\gamma)$ (eV)	Reference
χPTh, $\mathcal{O}(p^2)$	0	[2]
χPTh, $\cdots + \mathcal{O}(p^4)$	0.004	[2]
χPTh, $\cdots + \mathcal{O}(p^6)$	0.42 ± 0.20	[2]
χPTh, $\cdots + \mathcal{O}(p^6)$	0.47	[4]
χPTh, ENJL, $\cdots + \mathcal{O}(p^6)$	0.58 ± 0.30	[5]
χPTh, ENJL, $\cdots + \mathcal{O}(p^6)$	$0.27^{+0.18}_{-0.07}$	[6]
VMD	0.30 ± 0.15	[7]
Q box	0.70	[7]
χPTh, $\cdots + \mathcal{O}(p^6)$	0.44 ± 0.09	[8]
unitarized χPTh	0.47 ± 0.10	[9]

to be confirmed, it would be the first real failure of χPTh and give a major setback to nonperturbative QCD.

The Crystal Ball multiphoton spectrometer (CB) is uniquely suited for tackling the challenging $\eta \to \pi^0\gamma\gamma$ decay. We have obtained the CB on loan from SLAC, moved it to BNL, and installed it in the C6 π^- beam of the Alternating Gradient Synchrotron (AGS). A two-week run was devoted to investigating rare η-meson decays.

Because of the huge background from $\eta \to 3\pi^0$ decay and from the reaction $\pi^- p \to \pi^0\pi^0 n$, the extraction of the $\pi^0\gamma\gamma$ signal is complicated. So it was decided to make two independent analyses. The first one used the kinematic-fit technique for event reconstruction and selection, followed by a binned maximum-likelihood fit of the Monte-Carlo spectra to the experimental spectrum of the $\pi^0\gamma\gamma$ invariant mass. The preliminary result of this analysis, $\mathrm{BR}(\eta \to \pi^0\gamma\gamma) = (3.2 \pm 0.9) \times 10^{-4}$, was reported in 2001 at the NANP'01 conference [13] and also presented at the Eta Physics Workshop [14] in Uppsala. In the second analysis, the separation of signal from background was based on the log likelihood function that was used in maximum-likelihood fits, exploiting the difference in shape between probability distributions. This method was presented in detail in a Ph.D. thesis [15]. It yielded 121 ± 37 events that led to $\mathrm{BR}(\eta \to \pi^0\gamma\gamma) = (2.7 \pm 0.9_{\mathrm{stat}} \pm 0.8_{\mathrm{syst}}) \times 10^{-4}$. This result, with the systematic uncertainty reduced in half, was reported in a condensed form in Ref. [16].

In this paper, we present the final result of the expanded first analysis, which is based on the kinematic-fit technique and binned maximum-likelihood fits. It yields a signal of 1.6 thousand $\eta \to \pi^0\gamma\gamma$ events and $\mathrm{BR}(\eta \to \pi^0\gamma\gamma) = (3.5 \pm 0.7_{\mathrm{stat}} \pm 0.6_{\mathrm{syst}}) \times 10^{-4}$.

II. EXPERIMENTAL SETUP

The η's were produced in the reaction

$$\pi^- p \to \eta n \tag{1}$$

close to threshold. The CB consists of 672 optically isolated NaI(Tl) crystals, shaped like truncated, triangular pyramids and arranged in two hemispheres covering 93% of 4π steradians. The pulse height in every crystal was measured using a separate ADC. To register the timing information, a TDC was used for every minor triangle, which is a group of nine neighboring crystals. The typical energy resolution for electromagnetic showers in the CB was $\Delta E/E = 0.020/(E[\mathrm{GeV}])^{0.36}$. Shower directions were measured with a resolution in θ, the polar angle with respect to the beam axis, of $\sigma_\theta = 2^\circ - 3^\circ$ for photon energies in the range 50–500 MeV, assuming that the photons are produced in the center of the CB. The resolution in azimuthal angle ϕ is $\sigma_\phi = \sigma_\theta / \sin\theta$. The angular resolutions are defined mainly by the granularity of the CB.

The experiment used a momentum-analyzed beam of negative pions incident on a 10-cm-long liquid-hydrogen (LH_2) target located at the center of the CB. The mean value of the incident momentum spectrum at the center of the LH_2 target was 716 MeV/c, the momentum spread was $\sim$12 MeV/c, and the momentum resolution of an individual beam pion was $\sim$0.6%.

The beam signal was a coincidence between three scintillation counters located in the beam line upstream of the CB. The event signal was the beam signal in coincidence with a CB signal, which included the requirement that the total energy deposited in the crystals exceeded a threshold of 0.4 GeV. The high threshold suppresses triggering on the $\pi^- p \to \pi^0 n$ reaction, which has a total cross section that is four times larger than $\pi^- p \to \eta n$. The neutral-event trigger fulfills the requirement that signals from a barrel of scintillation counters surrounding the target were in anticoincidence with the CB event signal. More details about the CB detector can be found in Refs. [16–20].

III. OUTLINE OF ANALYSIS

We have obtained an ensemble of more than 75 million events on tape. They are mainly π^0 and $2\pi^0$ production events and neutral decays of the η. Each event carries its pertinent information on the momentum, direction in space, and time of arrival of the incident π^-. The main information is the energy deposited and time of arrival in every one of the 672 crystals of the CB. The signals in the CB were arranged in clusters that are groups of adjacent counters in which the energy deposited exceeded a certain threshold. The procedure is detailed in Ref. [17]. The events were grouped into different classes depending on cluster multiplicity.

To determine $\mathrm{BR}(\eta \to \pi^0\gamma\gamma)$ we need to know the number of η mesons produced. For this purpose we use our measured data set of $\eta \to 2\gamma$ events that is obtained simultaneously with the $\eta \to \pi^0\gamma\gamma$ data. The $\eta \to 2\gamma$ sample is found in the two-cluster class. Note that $\mathrm{BR}(\eta \to 2\gamma)$ is known to 0.7% [21]. The analysis of the $\eta \to 2\gamma$ events is done with a kinematic-fit technique similar to that for the $\eta \to \pi^0\gamma\gamma$ data. This provides us with an opportunity to show the high quality of our analysis. A valuable confirmation of the number of η's produced has been obtained from the analysis of six-cluster events from the $\pi^- p \to \eta n \to 3\pi^0 n \to 6\gamma n$ reaction.

The goal of our analysis is to find the number of $\eta \to \pi^0\gamma\gamma$ decays in such a way that we can calculate the detection efficiency. Since a π^0 decays promptly into 2γ with $\mathrm{BR} = 98.8\%$, the desired $\eta \to \pi^0\gamma\gamma$ events are four-photon events. The invariant mass of the four photons must be the mass

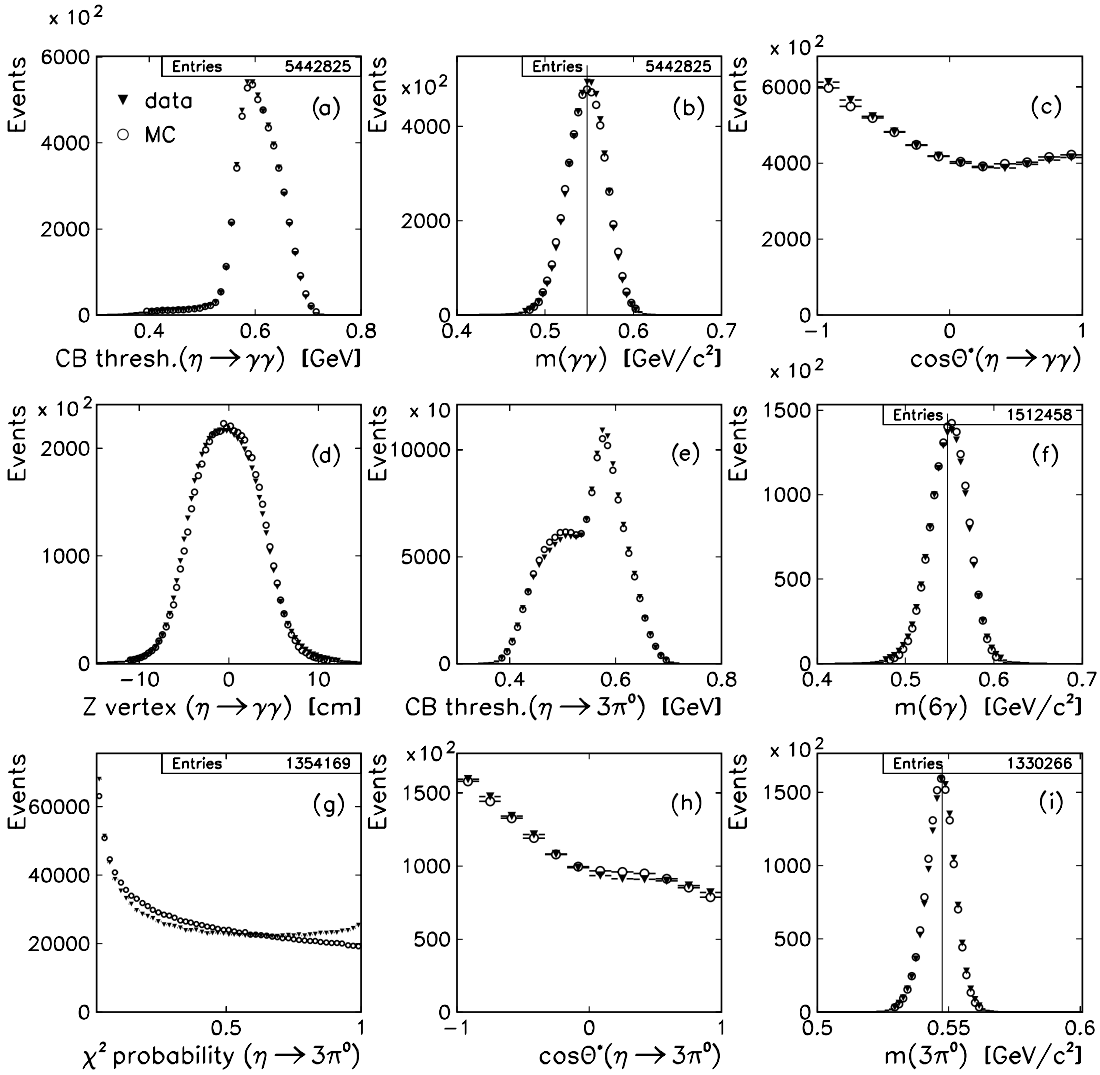

FIG. 1. Comparison of data (solid triangles) and MC (circles) distributions. For the two-cluster events satisfying the $\pi^- p \to \eta n \to \gamma\gamma n$ hypothesis we show (a) the CB energy threshold, (b) the two-photon invariant mass, (c) the c.m. η-production angle, and (d) the vertex z coordinate. For the six-cluster events satisfying the $\pi^- p \to \eta n \to 6\gamma n$ hypothesis we show (e) the CB energy threshold and (f) the six-photon invariant mass. For the six-cluster events satisfying the $\pi^- p \to \eta n \to 3\pi^0 n \to 6\gamma n$ hypothesis we show (g) the χ^2 probability of a 4-C kinematic fit, (h) the c.m. η-production angle, and (i) the $3\pi^0$ invariant mass. The vertical line in the invariant-mass spectra (b), (f), and (i) shows the η mass, which is 0.547 GeV/c^2 [21].

of the η, which is 0.547 GeV. The BR for $\eta \to \pi^0\gamma\gamma$ is small, of order a few times 10^{-4}. The backgrounds are high, e.g., the cross section for the four-photon reaction $\pi^- p \to \pi^0\pi^0 n$ is comparable to $\pi^- p \to \eta n$. The "dangerous" neutral η-decay modes into $3\pi^0$ and 2γ are a thousand times larger than the reaction under study. The approach that we have taken in our analysis is to keep as many good $\eta \to \pi^0\gamma\gamma$ candidates as possible while suppressing the major backgrounds. This has been achieved by applying several different cuts: some are traditional ones, and others are specific to this work. These cuts exploit the subtle differences in the kinematic features of the $\eta \to \pi^0\gamma\gamma$ decay and the background processes.

We employ the kinematic-fit technique. The data sample that remains after all selection cuts is the basis of the "ultimate" data spectrum, which is the invariant-mass spectrum of our $\pi^0\gamma\gamma$ candidates. This spectrum is then used to extract the number of $\eta \to \pi^0\gamma\gamma$ events by the binned maximum-likelihood technique that takes properly into account the statistical uncertainties of the spectra. These spectra involve the hydrogen-target and empty-target data sets and also sets of Monte Carlo (MC) simulations of $\eta \to \pi^0\gamma\gamma$ events and all important background reactions. The actual event extraction has been made for many different selection criteria. This is done to assess the importance of possible systematic uncertainties.

IV. DETERMINATION OF THE SIZE OF THE η SAMPLE

The CB is an especially suitable device for the measurement of neutral η decays because simultaneously with the desired

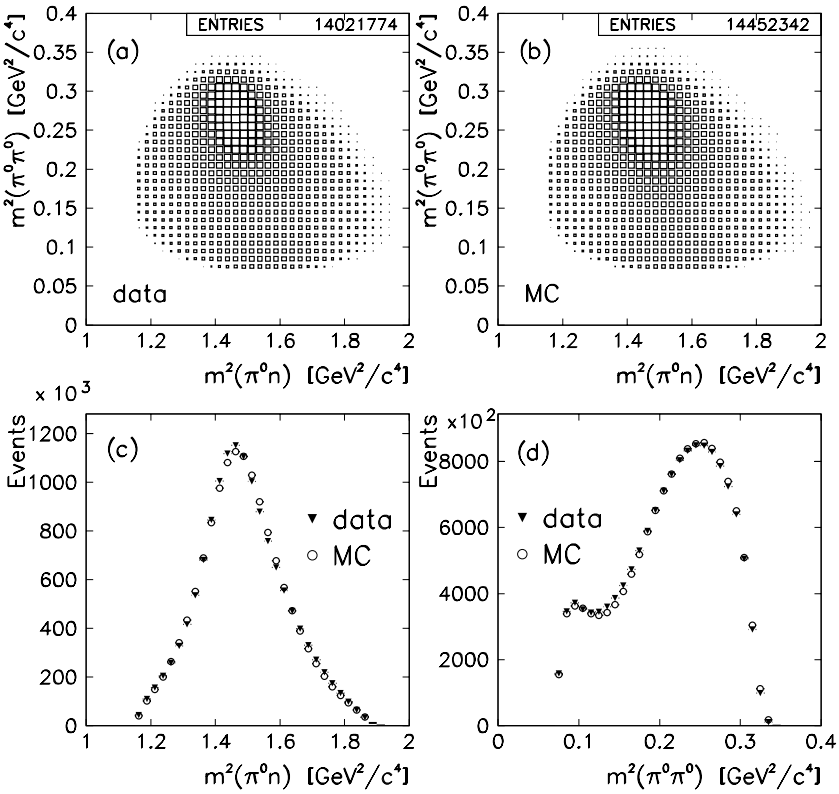

FIG. 2. Comparison of the data and MC distributions for reaction $\pi^- p \to \pi^0\pi^0 n$: (a) Dalitz plot of the data, (b) Dalitz plot of the MC simulation, (c) the $\pi^0 n$ invariant mass squared, and (d) the $\pi^0\pi^0$ invariant mass squared. The MC invariant mass spectra are normalized to the data.

η-decay mode, the CB also detects the well-known η-decay into 2γ (39.4%) and $3\pi^0$ (32.5%). These two decay modes are used to obtain the size of the total η sample. Furthermore, they enable us to make many useful checks on the analysis. The mean momentum of the incident π^- beam is 720 MeV/c. This is close to the η production threshold. In 95% of the cases, the recoil neutron from the $\pi^- p \to \eta n$ reaction escapes detection by the CB because it leaves the detector through the forward exit tunnel. Furthermore, the neutron detection efficiency of the CB for our energies is less than 30%. So in our analysis, we can neglect events in which there is an extra cluster from a neutron interaction in the CB.

The cluster algorithm was optimized for determining a group of neighboring crystals in which energy was deposited from a single-photon electromagnetic shower. The software threshold for the cluster energy was chosen to be 14 MeV, which optimizes the number of reconstructed $\pi^- p \to \eta n$ events.

Since the decay time of NaI (Tl) is about 250 ns, it is possible to find one or more clusters that do not belong to the event that generated the CB trigger. The fraction of these pile-up clusters increases when the beam intensity is increased. The pile-up clusters, unless they are eliminated, change the cluster multiplicity of good events. As a consequence, such events would be lost in the analysis. The elimination of the pile-up clusters is based on the TDC information of the crystals forming the clusters. All clusters that occur outside the proper TDC gate were eliminated from further consideration. Some small losses occur only if the true cluster overlaps with the pile-up one. From a comparison of the data samples taken at a different beam intensity, we deduced that these losses vary from zero to a few percent. Since our experiment is based on measuring relative branching ratios of the η, such losses are unimportant to us.

All two-cluster were subjected to a kinematic fit to test the $\pi^- p \to \eta n \to 2\gamma n$ hypothesis, and all six-cluster events were tested to the $\pi^- p \to \eta n \to 6\gamma n$ hypothesis. The measured parameters in the kinematic fit include five for the beam particle (momentum, angles θ_x and θ_y, and position coordinates x and y in the target) and three for each photon cluster (energy, angles θ and ϕ). Since the neutron was not detected, its energy and two angles were free parameters in the fit. The z coordinate of the vertex (i.e., the point where the η is produced and decayed) was also a free parameter of the kinematic fit. In addition to the four main constraints of the kinematic fit, which are based on energy and three-momentum conservation, there is one more constraint: the invariant mass of the final-state photons must be the known η-meson mass. The total number of constraints for both hypotheses is five. The effective number of constraints is smaller by the number of free parameters of the fit; thus we have a 1-C fit. The pulls of the kinematic fit for the beam, photon, and neutron variables were adjusted to agree with a normal distribution that has a mean value of zero and variance 1. A small deviation from the normal distribution occurs for events with a large cluster multiplicity, when some clusters overlap, or when a part of the electromagnetic shower leaks into the CB exit tunnel.

Events that satisfied the $\pi^- p \to \eta n \to 2\gamma n$ or $\pi^- p \to \eta n \to 6\gamma n$ hypothesis at the 2% confidence level (CL)

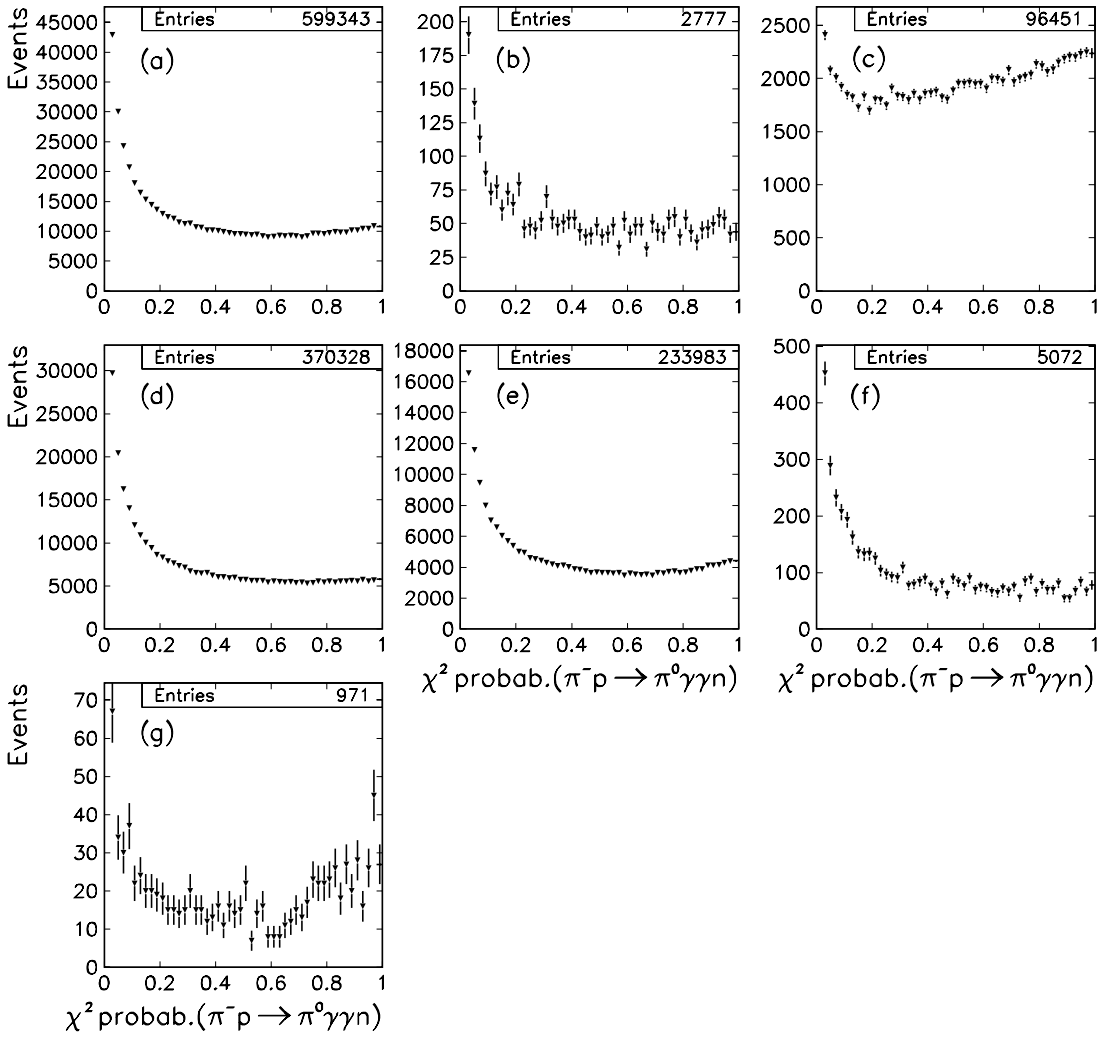

FIG. 3. The probability distributions for four-cluster events that survived the $2\pi^0$ cut and passed the 2% CL cut for the 1-C hypothesis $\pi^- p \to \pi^0\gamma\gamma n \to 4\gamma n$: (a) experimental LH_2 data, (b) experimental empty-target data, (c) MC simulation for 4×10^5 $\pi^- p \to \eta n \to \pi^0\gamma\gamma n$ events, (d) MC for 3×10^7 $\pi^- p \to \eta n \to 3\pi^0 n$ events, (e) MC for 4×10^7 $\pi^- p \to \pi^0\pi^0 n$ events, (f) MC for 1×10^7 $\pi^- p \to \eta n \to \gamma\gamma n$ events, and (g) MC for 6×10^6 $\pi^- p \to \pi^0 n$ events.

(i.e., with a probability greater than 2%) were accepted as the corresponding event candidates. A tighter cut on the CL is not necessary, as there is no physical background. The production of the $3\pi^0 n$ final state that does not originate as an η-decay is small at these energies [20], so we neglected this contribution. The only background that occurs is η production in target material different from LH_2. The fraction of this background was estimated using empty-target data samples. A 1-C fit yielded 5.443 M $\eta \to 2\gamma$ events at the 2% CL. The empty-target background in these events was found to be 2.22%. The corresponding number of $\eta \to 6\gamma$ events was 1.512 M, with 2.25% empty-target background. In addition, the $\eta \to 6\gamma$ events were subjected to a kinematic fit for testing the 4-C hypothesis $\pi^- p \to \eta n \to 3\pi^0 n \to 6\gamma n$ and the 3-C hypothesis $\pi^- p \to 3\pi^0 n \to 6\gamma n$. The kinematic fit was performed for each of the 15 possible pairing combination of six photons to form three π^0's. The pairing combination with the largest CL was used to reconstruct the kinematics of the processes.

A MC simulation of $\pi^- p \to \eta n$ was performed using the beam spectrum extracted for this reaction from the data. The angular distribution for $\pi^- p \to \eta n$ needed in the MC simulation was determined from the data as well. The simulation of the $\eta \to 3\pi^0$ and $\eta \to \pi^0\gamma\gamma$ decays was made according to phase space. Next, the MC events were propagated through a full GEANT (version 3.21) simulation of the CB detector, folded with the CB resolutions and trigger conditions, and analyzed the same way as the experimental data. Out of 10 M $\pi^- p \to \eta n \to \gamma\gamma n$ input MC events, 4.883 M fulfilled the $\pi^- p \to \eta n \to \gamma\gamma n$ hypothesis at the 2% CL. The seemingly low rate of acceptance, 48.8%, of our detector is due mainly to the escape of one of the two photons through the downstream exit tunnel, the size of which is effectively enhanced by the forward kinematic boost and to photons converting in the long veto-barrel counters. The systematic uncertainty in the $\pi^- p \to \eta n \to \gamma\gamma n$ acceptance, which is about 0.3%, is determined by the systematics of the MC simulation. Correcting 5.443 M experimental $\eta \to 2\gamma$

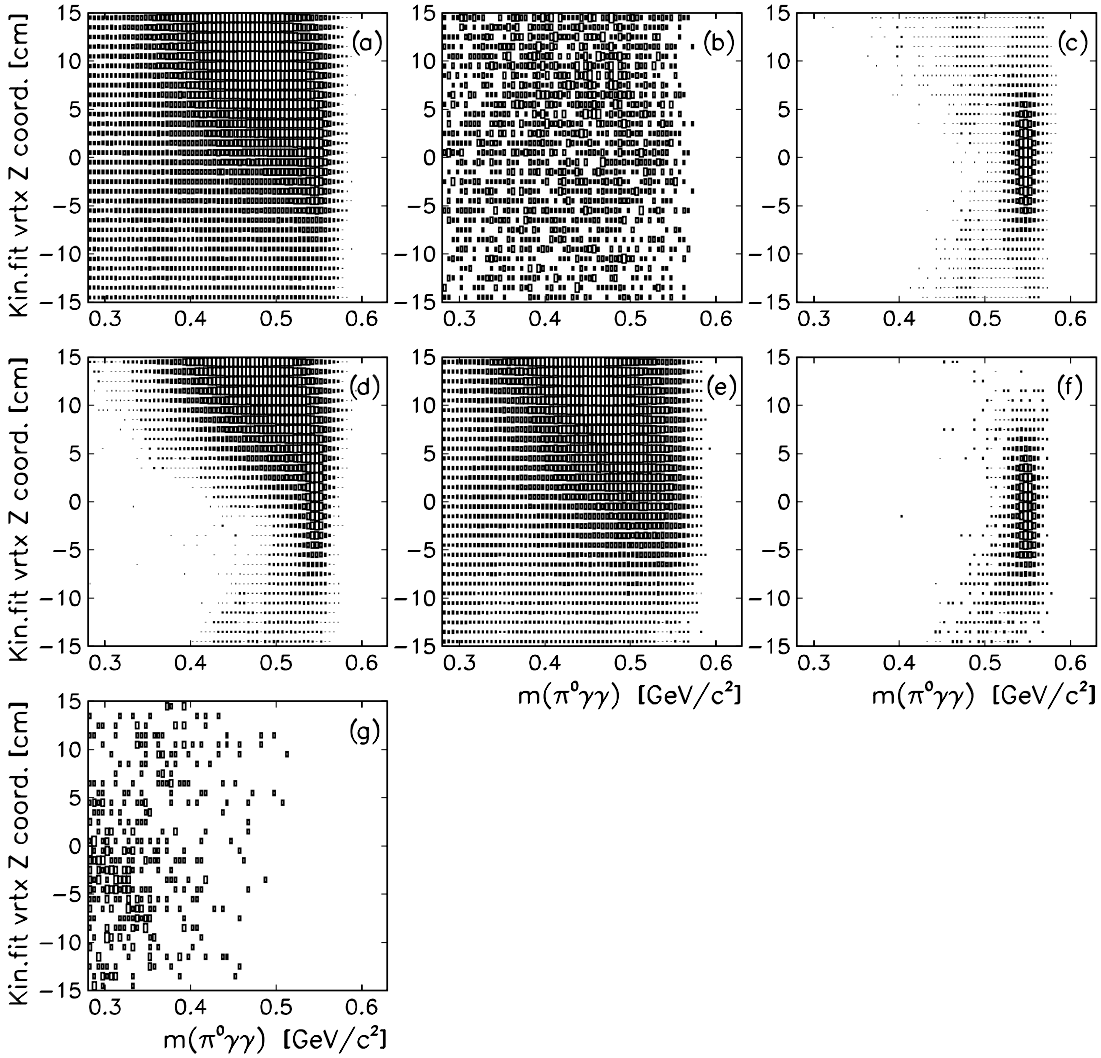

FIG. 4. Two-dimensional distributions of the vertex z coordinate versus the $\pi^0\gamma\gamma$ invariant mass, where both of the parameters are obtained from the output of the kinematic fit to the hypothesis $\pi^- p \to \pi^0\gamma\gamma n \to 4\gamma n$: (a) experimental LH_2 data, (b) experimental empty-target data, (c) MC simulation for $\pi^- p \to \eta n \to \pi^0\gamma\gamma n$, (d) MC for $\pi^- p \to \eta n \to 3\pi^0 n$, (e) MC for $\pi^- p \to \pi^0\pi^0 n$, (f) MC for $\pi^- p \to \eta n \to \gamma\gamma n$, and (g) MC for $\pi^- p \to \pi^0 n$.

events for the 2.22% empty-target background and the acceptance of 48.8%, we obtain 10.898 M $\eta \to 2\gamma$ original events. Taking the PDG value $\mathrm{BR}(\eta \to \gamma\gamma) = 0.3943 \pm 0.0026$ [21], the overall number of η mesons produced is (27.64 ± 0.25) M.

An independent evaluation of the η yield using the $\pi^- p \to \eta n \to 3\pi^0 n$ process was also performed. The MC acceptance for $\pi^- p \to \eta n \to 3\pi^0 n$ was determined to be 17.1%. of the six final state photons in the veto barrel and the downstream exit tunnel. The systematic uncertainty in the $\pi^- p \to \eta n \to 3\pi^0 n \to 6\gamma n$ acceptance, which is about 1%, is determined by the systematics of the MC simulation. Correcting the 1.512 M experimental $\eta \to 3\pi^0$ events for the empty-target background and the acceptance, we obtain 8.668 M $\eta \to 3\pi^0$ original events. Taking the PDG value $\mathrm{BR}(\eta \to 3\pi^0) = 0.3251 \pm 0.0029$ [21], the overall number of η mesons produced is (26.1 ± 1.5) M. The difference of 5.6% in the two methods comprises our systematic uncertainty in the determination of the number of η mesons produced.

In Fig. 1, we illustrate the agreement between data and the MC distributions obtained for the $\pi^- p \to \eta n$ reaction. Figure 1(a) compares the data and MC distributions for the threshold energy of the CB trigger obtained from two-cluster events selected as the $\pi^- p \to \eta n \to 2\gamma n$ process. For the same process, Figs. 1(b)–1(d) display the two-photon invariant mass spectrum, the distribution of the η-production angle in the overall center-of-mass (c.m.) system, and the distribution of the vertex z coordinate, which was a free parameter in the kinematic fit. In Figs. 1(e) and 1(f), we show the CB energy threshold and the six-photon invariant mass spectrum for events selected as the $\pi^- p \to \eta n \to 6\gamma n$ process. In Fig. 1(g), we compare the χ^2 probability distribution of the 4-C fit to the $\pi^- p \to \eta n \to 3\pi^0 n \to 6\gamma n$ hypothesis. The small disagreement between the data and the MC distributions reflects our limited knowledge of the uncertainties in the beam

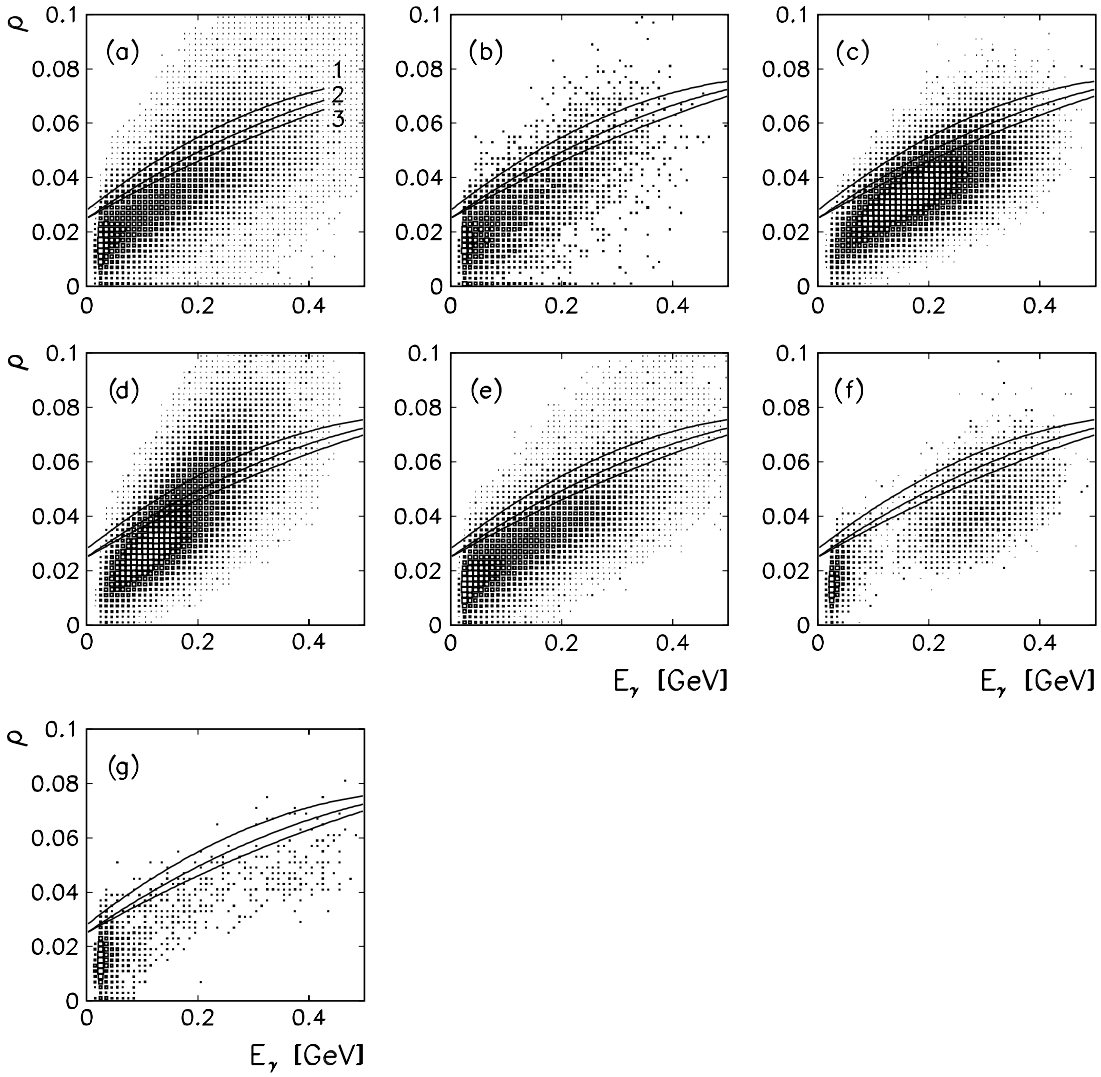

FIG. 5. Two-dimensional plots of the parameter ρ versus the cluster energy of each of the two photons from η-decay obtained for events selected as $\pi^- p \to \pi^0\gamma\gamma n \to 4\gamma n$ candidates: (a) experimental LH_2 data, (b) experimental empty-target data, (c) MC simulation for $\pi^- p \to \eta n \to \pi^0\gamma\gamma n$, (d) MC for $\pi^- p \to \eta n \to 3\pi^0 n$, (e) MC for $\pi^- p \to \pi^0\pi^0 n$, (f) MC for $\pi^- p \to \eta n \to \gamma\gamma n$, and (g) MC for $\pi^- p \to \pi^0 n$. The curves in the plots show the cuts on ρ. The cuts require discarding all events in which at least one value of ρ lies above the curve. The numbers that label the curves increase with tighter cut criteria.

momentum and ADC pedestals for the individual events of the experimental data. Note that the standard way for diminishing the systematic uncertainty due to applying a cut on the kinematic-fit CL is to not use a tight CL for the event selection. In Fig. 1(h), we compare the η-production angular distribution for six-cluster events selected as $\pi^- p \to \eta n \to 3\pi^0 n \to 6\gamma n$ at the 2% CL. Testing the $\pi^- p \to 3\pi^0 n \to 6\gamma n$ hypothesis, in which the constraint on the η mass is omitted, illustrates the improvement in the CB invariant mass resolution due to the application of a kinematic fit. In Fig. 1(i), we compare the $3\pi^0$ invariant mass distribution of the data and the MC simulation. Both the data and the MC simulation have identical invariant-mass resolution with $\sigma \approx 5$ MeV/c^2. Note the very good agreement in Fig. 1 between the experimental and MC distributions [except Fig. 1(g), which is not significant].

V. REDUCTION OF THE BACKGROUND REACTIONS

The four-cluster data sample was used to search for candidates of the

$$\pi^- p \to \eta n \to \pi^0\gamma\gamma n \to 4\gamma n \tag{2}$$

process. Since the sample of the $\eta \to \pi^0\gamma\gamma$ decays is expected to be very small, the major background contributions need to be suppressed prior to the final maximum-likelihood fittings of the event distributions. Also, all background processes must be properly simulated. The selection criteria were optimized to suppress background processes to the level where the number of expected events from process (2) was comparable to the number of background events in the η-mass region.

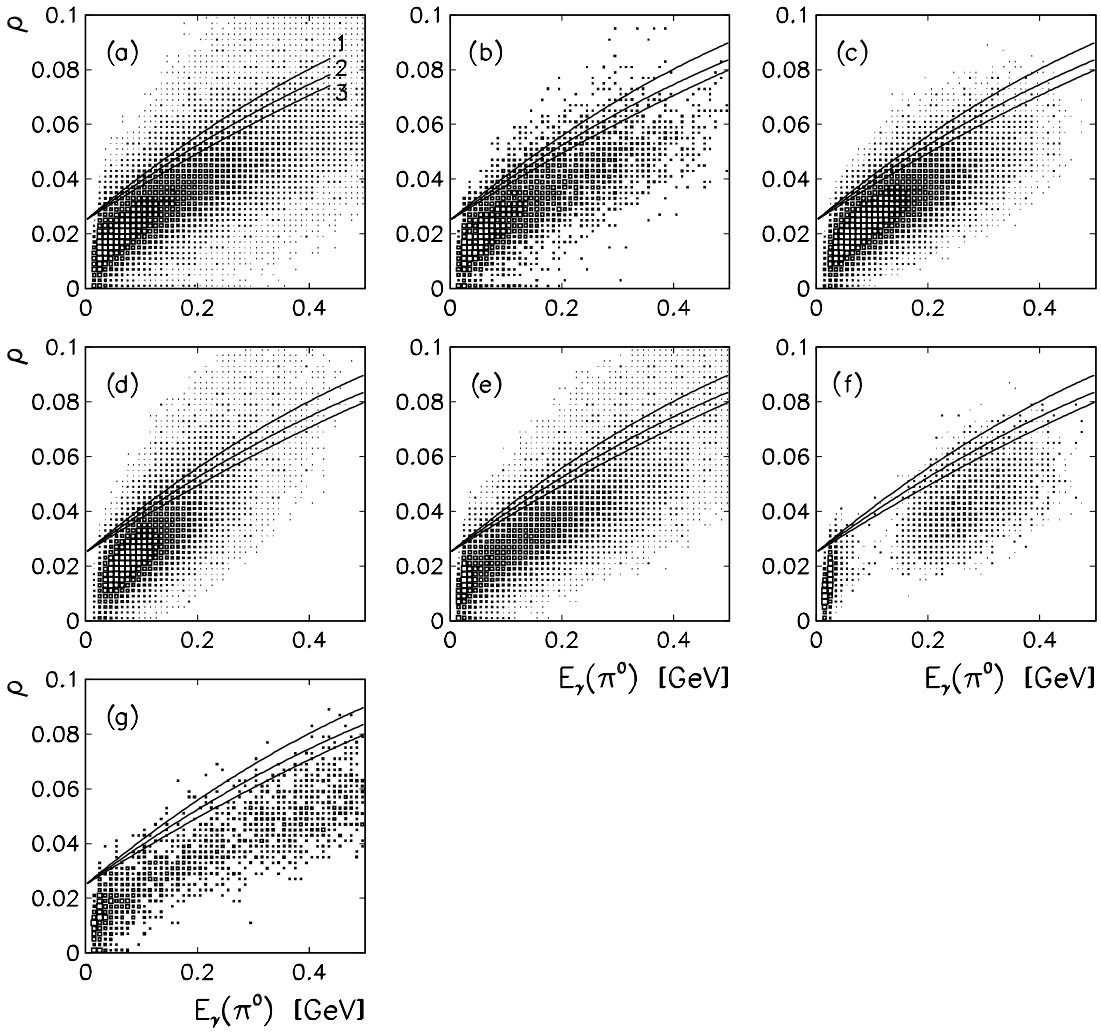

FIG. 6. Same as Fig. 5 when both photons are from the π^0 decay.

The largest contribution to the four-photon final state is due to the

$$\pi^- p \to \pi^0\pi^0 n \to 4\gamma n \tag{3}$$

process. These events do not produce a peak in the η-mass region; however, understanding the behavior of this background under the η peak is important for the correct determination of the $\eta \to \pi^0\gamma\gamma$ signal. The kinematics of the $\pi^- p \to \pi^0\pi^0 n$ reaction have been studied separately by us with the CB [17]. It was found that the Dalitz plot is highly nonuniform and changes dramatically for different directions of the recoil neutron. For the realistic description of this background, a MC based on phase space is not acceptable. Because of the lack of a reliable full model for $\pi^- p \to \pi^0\pi^0 n$, we used the experimentally measured distributions for our simulation. The $\pi^- p \to \pi^0\pi^0 n$ reaction was simulated using the beam spectrum determined for this reaction from the data. The dynamics of the reaction were simulated as the $\pi^- p \to \pi^0\Delta(1232) \to \pi^0\pi^0 n$ process with other features (like production and decay angular distributions) corresponding to the ones measured by us and reported in Ref. [17]. In Fig. 2, we compare the data and MC distributions for events of the $\pi^- p \to \pi^0\pi^0 n$ reaction selected by the kinematic fit at the 2% CL. Figures 2(a) and 2(b) show the Dalitz plot obtained for the data and the MC simulation. In Figs. 2(c) and 2(d), we compare the Dalitz-plot projections of the $\pi^0 n$ and $\pi^0\pi^0$ invariant mass squared, where the MC spectra are normalized to the data.

The background due to $\eta \to 2\gamma$ and $\eta \to 3\pi^0$ events is particularly dangerous, because it has a fake peak at the η mass. The $\eta \to 2\gamma$ events contribute to our four-cluster sample mostly when both the photons produce split-off showers, and the invariant mass of any two clusters is close to the π^0-meson mass. The $\eta \to 3\pi^0$ background events occur when final-state photons produce overlapping clusters or escape through the CB exit tunnel. The agreement of the data and the MC simulation for the processes $\pi^- p \to \eta n \to \gamma\gamma n$ and $\pi^- p \to \eta n \to 3\pi^0 n \to 6\gamma n$ is illustrated in Fig. 1.

A four-cluster event can even occur due to the reaction $\pi^- p \to \pi^0 n$ when two extra clusters come from photon shower split-offs and/or neutron interactions in the CB. The events from this background usually lie below the η-mass region. The MC simulation of this background was performed,

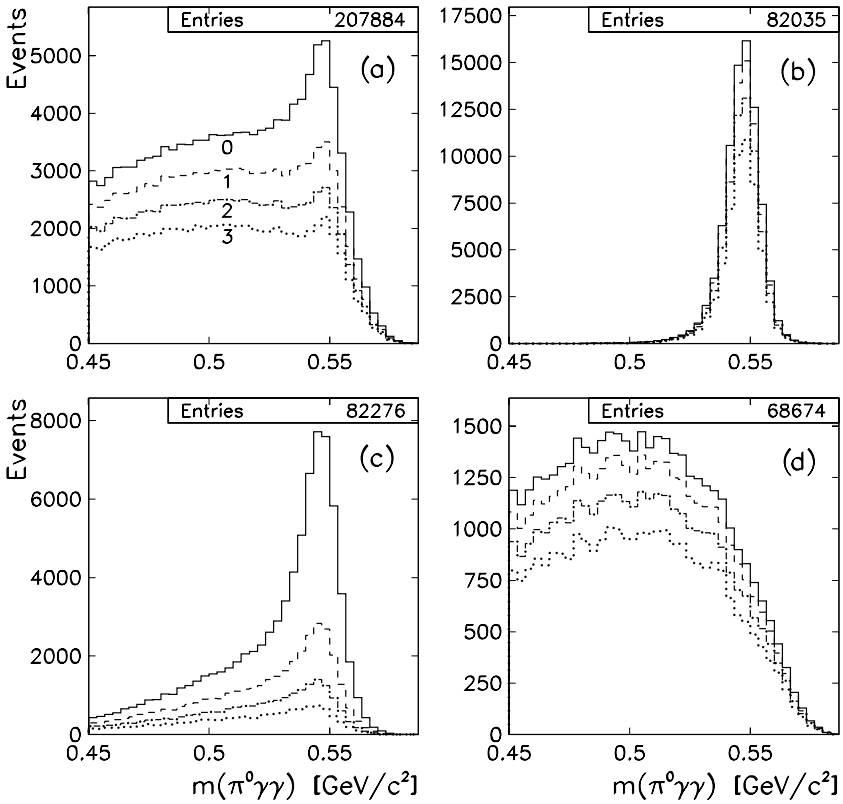

FIG. 7. Change of the $\pi^0\gamma\gamma$ invariant-mass spectrum upon applying different ρ cuts: (a) experimental LH_2 data, (b) MC simulation for $\pi^- p \to \eta n \to \pi^0\gamma\gamma n$, (c) MC for $\pi^- p \to \eta n \to 3\pi^0 n$, and (d) MC for $\pi^- p \to \pi^0\pi^0 n$. The spectra shown by the solid line (labeled No. 0) are obtained without any cut on ρ. The numbers that label the three other spectra correspond to the ρ-cut numbers shown in Figs. 5 and 6.

incorporating the features of $\pi^- p \to \pi^0 n$ measured by us using the same data sets.

The last source of background is the empty-target contribution which originates in pion beam interactions in the target walls or the passage through the CB of a μ^- from a π^- decay. Based on the analysis of the empty-target sample and the MC simulation for the process $\pi^- p \to \eta n \to \pi^0\gamma\gamma n$, almost all four-cluster events from μ^-'s were eliminated without affecting the $\eta \to \pi^0\gamma\gamma$ signal. The cut applied is based on the fact that all clusters produced by a μ^- have approximately the same ϕ angle. The remaining empty-target events are mostly due to π^0, $2\pi^0$, and η production on the nuclei of the material surrounding the liquid hydrogen. Note that suppression of such events using a kinematic fit is not very effective, since the proton mass is used as the hypothesis for the target, instead of an unknown nuclear mass. The subtraction of the empty-target background is made with the weight equal to the ratio of the beam pions incident on the full and the empty target. For this experiment, this ratio was determined to be 29.2. The systematic uncertainty in this ratio is 0.3. Despite the much lower statistics of the empty-target spectra compared to those of the full target, it is still sufficient for fitting one-dimensional histograms with the binned maximum-likelihood method.

As the first step in the analysis, we suppressed the large background from $\pi^- p \to \pi^0\pi^0 n$. For that purpose, all four-cluster events that satisfied the kinematic-fit hypothesis $\pi^- p \to \pi^0\pi^0 n \to 4\gamma n$ with a probability greater than 0.01% were removed. The $\pi^- p \to \pi^0\pi^0 n$ events can still contribute to the four-cluster sample when the neutron is detected and one of the photons escapes detection in the CB. Based on the MC simulation, we conclude that the test of the $\pi^- p \to \pi^0\gamma n \to 3\gamma n$ hypothesis removes most of this background. The test of the same hypothesis is useful for suppressing the $\pi^- p \to \pi^0 n$ background events in which one photon produces a split-off shower. Therefore, all events that satisfied this hypothesis with probability greater than 0.01% were not considered further. The remaining $\pi^- p \to \pi^0\pi^0 n$ background is mostly from events that show up in the tails of the experimental resolutions; i.e., when the reconstructed invariant mass of two decay photons from one of the two π^0's is far from the π^0-meson mass.

For the next step, all events that survived the $2\pi^0$ cut were tested for the 1-C hypothesis $\pi^- p \to \pi^0\gamma\gamma n \to 4\gamma n$. The resulting distributions for the kinematic fit probability are shown in Fig. 3 for the experimental data sets and for different MC-simulation sets that are based on samples of 4×10^5 $\pi^- p \to \eta n \to \pi^0\gamma\gamma n$ events, 3×10^7 $\pi^- p \to \eta n \to 3\pi^0 n$ events, 4×10^7 $\pi^- p \to \pi^0\pi^0 n$ events, 1×10^7 $\pi^- p \to \eta n \to \gamma\gamma n$ events, and 6×10^6 $\pi^- p \to \pi^0 n$ events. Note that the small dip in the probability distribution, near 0.2, for the process $\pi^- p \to \eta n \to \pi^0\gamma\gamma n \to 4\gamma n$ is caused by the aforementioned selection cuts imposed to suppress the $\pi^- p \to \pi^0\pi^0 n$ background. The probability distributions shown in Fig. 3 indicate that tightening the cut on the confidence level increases the ratio of signal to background processes only in the CL range below 20%.

The events that satisfied the above hypothesis at the 2% CL were used to make two-dimensional plots of the vertex z coordinate versus the $\pi^0\gamma\gamma$ invariant mass, where both parameters, z and $m(\pi^0\gamma\gamma)$, are obtained from the kinematic fit. These plots are shown in Fig. 4; they reveal that further

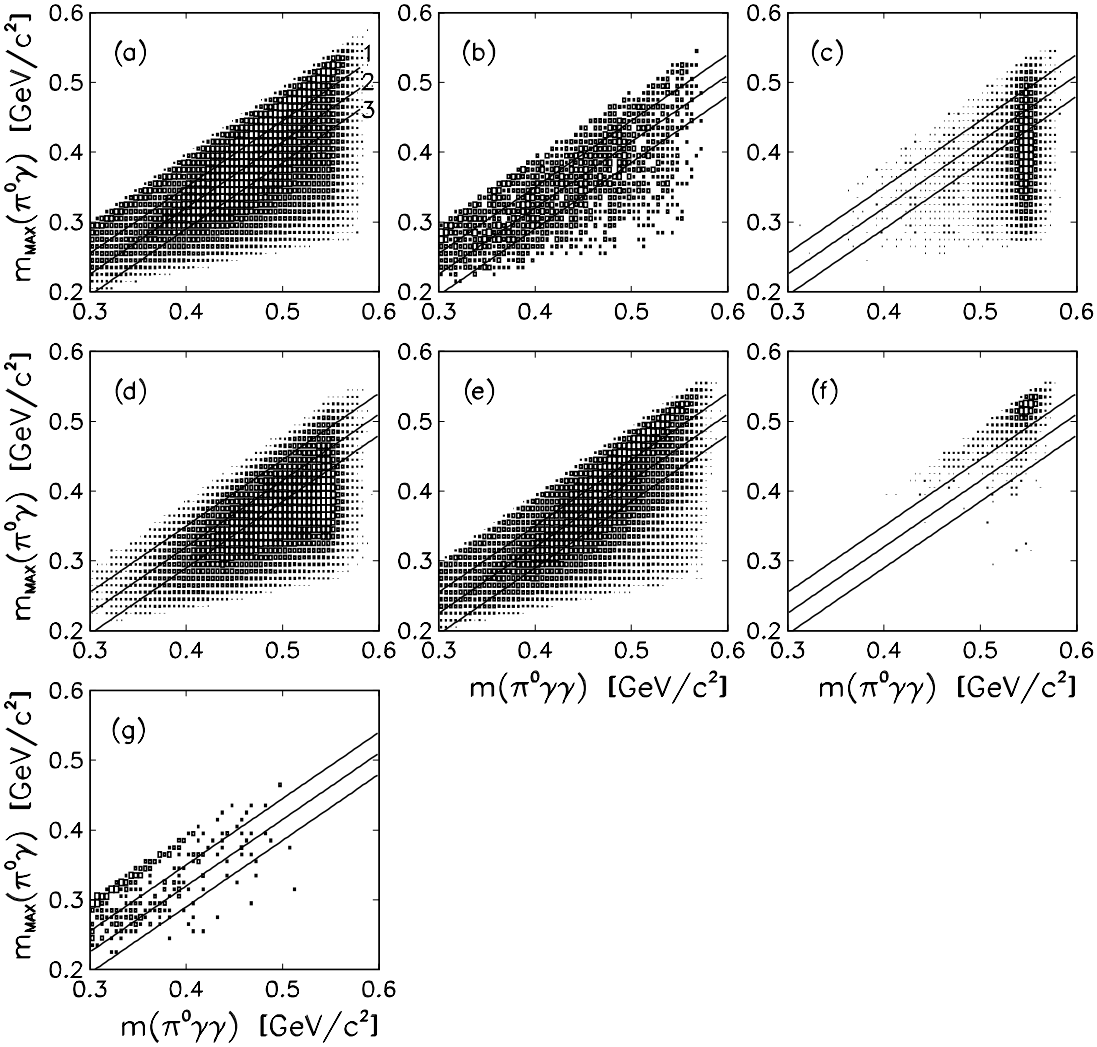

FIG. 8. Two-dimensional plots of the maximal $m(\pi^0\gamma)$ invariant mass (from the two possible ones) versus $m(\pi^0\gamma\gamma)$ for events selected as $\pi^- p \to \pi^0\gamma\gamma n \to 4\gamma n$ candidates: (a) experimental LH_2 data, (b) experimental empty-target data, (c) MC simulation for $\pi^- p \to \eta n \to \pi^0\gamma\gamma n$, (d) MC for $\pi^- p \to \eta n \to 3\pi^0 n$, (e) MC for $\pi^- p \to \pi^0\pi^0 n$, (f) MC for $\pi^- p \to \eta n \to \gamma\gamma n$, and (g) MC for $\pi^- p \to \pi^0 n$. The lines in the plots show the cuts on $m_{\max}(\pi^0\gamma)$. The cuts require discarding all events in which $m_{\max}(\pi^0\gamma)$ lies above the line. The number that labels the lines in (a) increases when the cut criteria are tighter.

improvement in the signal/background ratio can be achieved by tightening the cut on the vertex z coordinate. Note that usually for background reactions, the kinematic fit output for the vertex z coordinate has little in common with real pion-beam interactions in the target. In our analysis, we tested cases for a vertex z cut of $\pm 8, \pm 7, \pm 6$, and ± 5 cm. It is seen in Fig. 4(g) that the $\pi^- p \to \pi^0 n$ background events are located in the area below the η-meson mass. Based on this, the $\pi^- p \to \pi^0 n$ MC histograms were omitted in the binned maximum-likelihood fits, and all fits were performed with the cut $m(\pi^0\gamma\gamma) > 0.44$ MeV/c^2.

Since the $\eta \to 3\pi^0$ background in the η-mass region occurs mostly due to overlapping clusters, their radii should be systematically larger than for the normal single-photon clusters. To suppress this background, we used a cut on the so-called effective radius of clusters. We define the effective radius R of a cluster containing k crystals with energy E_i (in GeV) deposited above a certain threshold in crystal i as

$$R = \sqrt{\sum_i^k E_i \cdot (\Delta r_i)^2 \Big/ \sum_i^k E_i}, \tag{4}$$

where Δr_i is the opening angle (in radians) between the cluster direction and the crystal axis. For event selection, we found it more convenient to use cuts on parameter ρ defined as $\rho = R \cdot \sqrt{E}$, where E is the cluster energy. For events selected as $\pi^- p \to \pi^0\gamma\gamma n \to 4\gamma n$ candidates, Fig. 5 shows the experimental and MC-simulation plots of the ρ parameter versus the cluster energy obtained for each of two photons that are produced directly from the η decay. In Fig. 6, we show the same plots for each of the two photons from the π^0 decay. The curves in the plots are the effective radius cuts. The cuts are such that they discard all events for which at least one value of

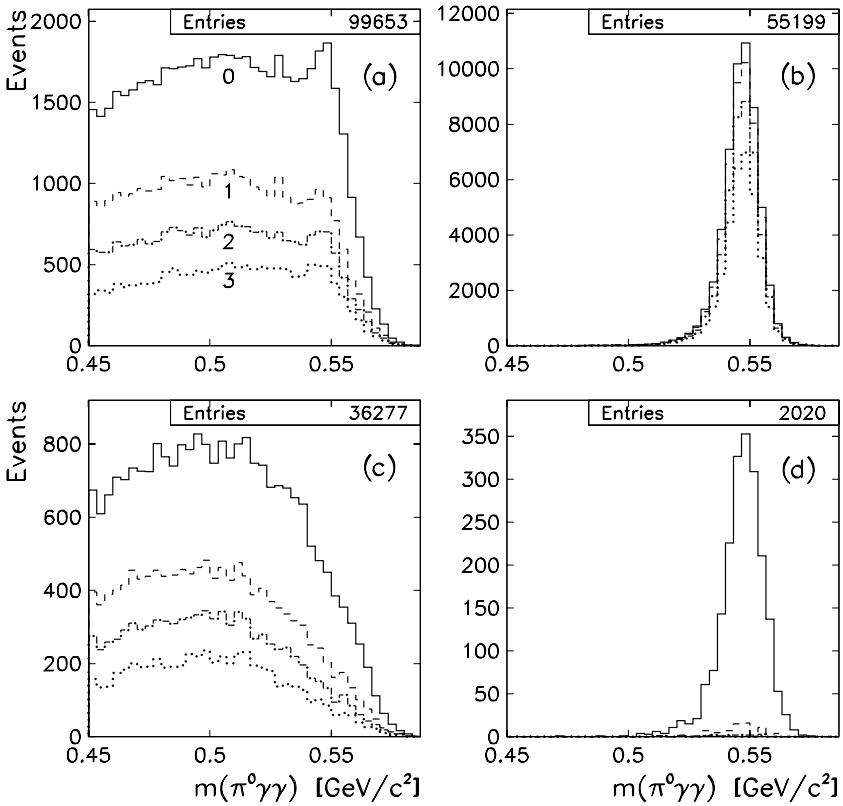

FIG. 9. Change of the $\pi^0\gamma\gamma$ invariant-mass spectrum upon applying different $m_{\max}(\pi^0\gamma)$ cuts: (a) experimental LH_2 data, (b) MC simulation for $\pi^- p \to \eta n \to \pi^0\gamma\gamma n$, (c) MC for $\pi^- p \to \pi^0\pi^0 n$, and (d) MC for $\pi^- p \to \eta n \to \gamma\gamma n$. The spectra shown by the solid line (labeled No. 0) are obtained without any cut on $m_{\max}(\pi^0\gamma)$. The numbers that label the three other spectra correspond to the $m_{\max}(\pi^0\gamma)$-cut numbers of Fig. 8.

ρ is above the curve. Several cuts were tested. The numbers (1, 2, or 3) that label the curves shown in Figs. 5 and 6 increase with tighter cut criteria. In order to prove the general case that there is no systematic difference between the effective radii of clusters calculated for the experimental and for the MC-simulation events, we compared the ρ distribution for the experimental four-cluster events identified as $\pi^- p \to \pi^0\pi^0 n$ and for the MC simulation of this reaction. No difference was found.

Figure 7 illustrates the change in the $\pi^0\gamma\gamma$ invariant-mass spectrum upon applying different ρ cuts. The spectra shown are for the experimental and MC-simulation events selected at the 2% CL and the vertex z coordinate within ± 6 cm. As can be seen in Fig. 7, the ρ cut dramatically improves the ratio of the $\eta \to \pi^0\gamma\gamma$ signal to the $\eta \to 3\pi^0$ background.

The $\pi^- p \to \pi^0\pi^0 n$ and $\eta \to \gamma\gamma$ background was suppressed by applying a cut on the two-dimensional plot of the largest $m(\pi^0\gamma)$ invariant mass (of the two possible ones) versus the $m(\pi^0\gamma\gamma)$ invariant mass. All invariant masses are calculated from the kinematic-fit results to the $\pi^- p \to n\pi^0\gamma\gamma \to n4\gamma$ hypothesis. In Fig. 8, we show the distributions for the experimental and MC-simulation events. The lines in the plots show several cuts that were tested. The cuts require discarding all events in which $m_{\max}(\pi^0\gamma)$ lies above the line. The numbers that label the lines increase with tighter cut criteria. As can be seen in Fig. 8, tightening the cut rejects almost all $\eta \to \gamma\gamma$ background. However, a considerable part of the $\eta \to \pi^0\gamma\gamma$ signal is cut off as well. Since the density distribution of $\eta \to \pi^0\gamma\gamma$ events in this plot depends on the matrix element for the decay amplitude, tightening this cut can result in an increase in the systematic uncertainty of the measurement.

Figure 9 illustrates the change in the $\pi^0\gamma\gamma$ invariant-mass spectrum upon applying different $m_{\max}(\pi^0\gamma)$ cuts. Spectra are shown for the experimental and MC-simulation events selected at the 20% CL, with $|z| \leqslant 6$ cm, and using ρ cut No. 2. The spectra shown by the solid line were obtained without any cut on $m_{\max}(\pi^0\gamma)$. The numbers that label the three other spectra correspond to the $m_{\max}(\pi^0\gamma)$-cut numbers from Fig. 8. As one can see in Fig. 9, the $m_{\max}(\pi^0\gamma)$ cut improves the ratio of the $\eta \to \pi^0\gamma\gamma$ signal to the $\pi^- p \to \pi^0\pi^0 n$ background, and dramatically suppresses the $\eta \to \gamma\gamma$ background.

VI. DETERMINATION OF BR($\eta \to \pi^0\gamma\gamma$) AND THE EVALUATION OF THE SYSTEMATIC UNCERTAINTY

The yield of $\eta \to \pi^0\gamma\gamma$ events was obtained from the fits of the $\pi^0\gamma\gamma$ invariant-mass spectra after various cuts have been made. The fit of the empty-target and MC-simulation spectra to the experimental LH_2 spectrum was performed with the HMCMLL routine [22], which uses a binned maximum-likelihood technique that takes properly into account the statistical uncertainties of both the experimental and MC spectra. We limit our fit to the invariant-mass range $m(\pi^0\gamma\gamma) > 0.44$ GeV/c^2. This cut eliminates almost all background from the $\pi^- p \to \pi^0 n$ events, so their spectrum is not included in the fits. Examples of $m(\pi^0\gamma\gamma)$ spectra obtained for four different sets of the selection cuts and the results of the binned maximum-likelihood fit for the yield of $\eta \to \pi^0\gamma\gamma$ events are shown in Figs. 10–13.

The weight factors of the empty-target, $\eta \to \gamma\gamma$, and $\eta \to 3\pi^0$ background spectra were fixed parameters of the

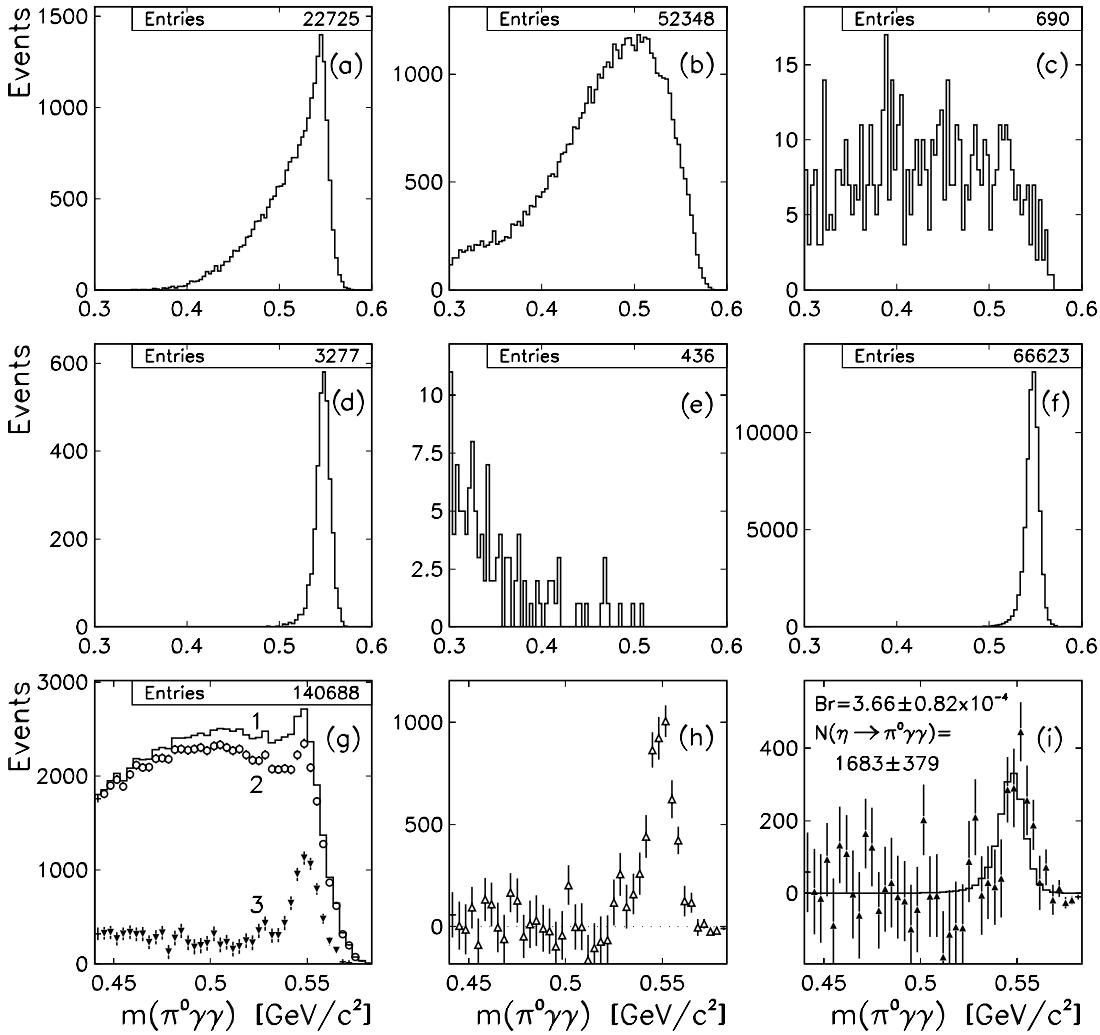

FIG. 10. Fit of the $m(\pi^0\gamma\gamma)$ spectra for the $\pi^- p \to \pi^0\gamma\gamma n$ candidates selected at the 2% CL, with the vertex z coordinate within ± 6 cm, and after applying cut No. 2 on the ρ parameter. (a) MC simulation for 3×10^7 $\pi^- p \to \eta n \to 3\pi^0 n$ events, (b) MC for 4×10^7 $\pi^- p \to \pi^0\pi^0 n$ events, (c) empty-target data, (d) MC for 1×10^7 $\pi^- p \to \eta n \to \gamma\gamma n$ events, (e) MC for 6×10^6 $\pi^- p \to \pi^0 n$ events (not used in the fit), (f) MC for 4×10^5 $\pi^- p \to \eta n \to \pi^0\gamma\gamma n$ events, (g) experimental LH_2 data before (spectrum No. 1) and after the $\eta \to 3\pi^0$ and the $\pi^0\pi^0$ background subtraction (spectrum No. 2 is the $\eta \to 3\pi^0$ subtraction only, spectrum No. 3 is after subtraction of both background contributions), (h) the remaining distribution after subtraction of the empty-target background from spectrum No. 3, and (i) final spectrum after subtraction of the $\eta \to \gamma\gamma$ background. The MC-simulation spectrum for $\eta \to \pi^0\gamma\gamma$, shown in (i) by the solid line, is normalized to the number of events for this process obtained from the fit.

maximum-likelihood fits. The weight factor of the empty target is 29.2, which is the ratio of the beam pions incident on the full and the empty target. The subtraction of the empty target background increases significantly the statistical uncertainties.

The weight factor for the $\eta \to \gamma\gamma$ background was fixed as the ratio of the number of the $\pi^- p \to \eta n \to \gamma\gamma n$ events measured experimentally to the number of MC simulated events for this process. Comparing the fit results for different cuts on $m_{\max}(\pi^0\gamma)$, we are able to investigate the systematic uncertainty generated by this choice of the weight factor. This uncertainty was found to be small.

In Ref. [23] we show in detail that the features of the $\eta \to 3\pi^0$ background in the four-cluster sample are very similar to features of the five-cluster sample. This background occurs when some of the six final-state photons are not detected because they leave in the direction of the CB beam tunnel, or when there are overlapping photon clusters. The advantage of the five-cluster sample as a test of how well the MC simulation reproduces the $\eta \to 3\pi^0$ background is that only three processes contribute to five-cluster multiplicity: $\pi^- p \to \eta n \to 3\pi^0 n$, $\pi^- p \to \pi^0\pi^0 n$, and the empty-target contribution. An analysis of the five-cluster sample showed that, depending on selection cuts, the fraction of the $\eta \to 3\pi^0$ background events varies between the value expected from our experimental number for the $\pi^- p \to \eta n \to 6\gamma n$ events observed and the value expected from our number of $\pi^- p \to \eta n \to 2\gamma n$ events times the PDG ratio, $\mathrm{BR}(\eta \to 3\pi^0)/\mathrm{BR}(\eta \to \gamma\gamma) = 0.825$. Based on the five-cluster sample analysis, the weight factor of the $\eta \to 3\pi^0$ background spectrum was fixed in the fits according to the average of the

TABLE II. The results for BR($\eta \to \pi^0\gamma\gamma$) obtained from the binned maximum-likelihood fits of $m(\pi^0\gamma\gamma)$ spectra for different cuts on the vertex z-coordinate limits, kinematic-fit CL, $\eta \to 3\pi^0$ (or parameter ρ), and $\pi^0\pi^0/\eta \to 2\gamma$ [or $m_{\max}(\pi^0\gamma)$]. The cases marked by an asterisk are illustrated in Figs. 10–13.

BR($\eta \to \pi^0\gamma\gamma$)[$\times 10^4$] with cuts	$\lvert Z_V\rvert < 8$ cm	$\lvert Z_V\rvert < 7$ cm	$\lvert Z_V\rvert < 6$ cm	$\lvert Z_V\rvert < 5$ cm
CL = 2%	4.57 ± 1.03	4.16 ± 0.99	3.56 ± 1.01	3.44 ± 1.02
CL = 5%	4.54 ± 0.88	4.22 ± 0.98	3.66 ± 1.00	3.66 ± 1.00
CL = 10%	4.36 ± 0.93	4.02 ± 1.00	3.52 ± 0.98	3.52 ± 1.00
CL = 20%	4.78 ± 1.02	4.36 ± 0.90	3.77 ± 1.01	3.71 ± 0.94
CL = 2%, No. $1_{\eta\to 3\pi^0}$	3.86 ± 0.90	3.65 ± 0.96	3.13 ± 0.83	3.07 ± 0.96
CL = 2%, No. $2_{\eta\to 3\pi^0}$	4.47 ± 0.89	4.29 ± 0.95	$3.66 \pm 0.82^*$	3.37 ± 0.86
CL = 2%, No. $3_{\eta\to 3\pi^0}$	4.45 ± 1.07	4.29 ± 0.90	3.72 ± 1.03	3.44 ± 1.07
CL = 2%, No. $1_{2\pi^0,\eta\to 2\gamma}$	4.50 ± 0.84	4.18 ± 0.77	3.55 ± 0.85	3.64 ± 0.85
CL = 2%, No. $2_{2\pi^0,\eta\to 2\gamma}$	4.44 ± 0.71	4.02 ± 0.67	3.46 ± 0.85	3.38 ± 0.85
CL = 2%, No. $3_{2\pi^0,\eta\to 2\gamma}$	3.86 ± 0.81	3.40 ± 0.71	3.07 ± 0.82	2.99 ± 0.90
CL = 2%, No. $1_{\eta\to 3\pi^0}$, No. $1_{2\pi^0,\eta\to 2\gamma}$	3.82 ± 0.79	3.72 ± 0.64	3.15 ± 0.76	3.30 ± 0.77
CL = 2%, No. $1_{\eta\to 3\pi^0}$, No. $2_{2\pi^0,\eta\to 2\gamma}$	4.01 ± 0.74	3.74 ± 0.72	3.25 ± 0.65	3.27 ± 0.67
CL = 2%, No. $1_{\eta\to 3\pi^0}$, No. $3_{2\pi^0,\eta\to 2\gamma}$	3.52 ± 0.76	3.22 ± 0.68	2.89 ± 0.76	2.91 ± 0.69
CL = 2%, No. $2_{\eta\to 3\pi^0}$, No. $1_{2\pi^0,\eta\to 2\gamma}$	4.58 ± 0.74	4.50 ± 0.71	3.89 ± 0.74	3.72 ± 0.77
CL = 2%, No. $2_{\eta\to 3\pi^0}$, No. $2_{2\pi^0,\eta\to 2\gamma}$	4.67 ± 0.69	4.47 ± 0.66	3.98 ± 0.67	3.85 ± 0.56
CL = 2%, No. $2_{\eta\to 3\pi^0}$, No. $3_{2\pi^0,\eta\to 2\gamma}$	4.16 ± 0.68	3.95 ± 0.65	3.67 ± 0.64	3.60 ± 0.57
CL = 20%, No. $1_{\eta\to 3\pi^0}$	3.74 ± 0.99	3.50 ± 0.99	2.99 ± 0.85	3.07 ± 0.81
CL = 20%, No. $2_{\eta\to 3\pi^0}$	4.22 ± 0.88	3.99 ± 0.99	$3.34 \pm 1.02^*$	3.25 ± 1.04
CL = 20%, No. $3_{\eta\to 3\pi^0}$	4.25 ± 1.11	3.99 ± 1.07	3.50 ± 1.07	3.50 ± 1.09
CL = 20%, No. $1_{2\pi^0,\eta\to 2\gamma}$	4.59 ± 0.85	4.22 ± 0.83	3.54 ± 0.85	3.49 ± 0.86
CL = 20%, No. $2_{2\pi^0,\eta\to 2\gamma}$	4.75 ± 0.81	4.28 ± 0.79	3.66 ± 0.82	3.54 ± 0.85
CL = 20%, No. $3_{2\pi^0,\eta\to 2\gamma}$	4.21 ± 0.72	3.83 ± 0.82	3.35 ± 0.67	3.20 ± 0.70
CL = 20%, No. $1_{\eta\to 3\pi^0}$, No. $1_{2\pi^0,\eta\to 2\gamma}$	3.64 ± 0.74	3.49 ± 0.67	2.93 ± 0.70	3.02 ± 0.69
CL = 20%, No. $1_{\eta\to 3\pi^0}$, No. $2_{2\pi^0,\eta\to 2\gamma}$	3.95 ± 0.68	3.66 ± 0.72	3.16 ± 0.75	3.17 ± 0.78
CL = 20%, No. $1_{\eta\to 3\pi^0}$, No. $3_{2\pi^0,\eta\to 2\gamma}$	3.56 ± 0.73	3.35 ± 0.67	3.00 ± 0.68	3.03 ± 0.51
CL = 20%, No. $2_{\eta\to 3\pi^0}$, No. $1_{2\pi^0,\eta\to 2\gamma}$	4.16 ± 0.78	3.99 ± 0.77	$3.41 \pm 0.79^*$	3.31 ± 0.83
CL = 20%, No. $2_{\eta\to 3\pi^0}$, No. $2_{2\pi^0,\eta\to 2\gamma}$	4.29 ± 0.72	4.04 ± 0.71	$3.60 \pm 0.73^*$	3.59 ± 0.72
CL = 20%, No. $2_{\eta\to 3\pi^0}$, No. $3_{2\pi^0,\eta\to 2\gamma}$	3.72 ± 0.73	3.55 ± 0.71	3.27 ± 0.69	3.28 ± 0.68
CL = 10%, No. $2_{\eta\to 3\pi^0}$, No. $1_{2\pi^0,\eta\to 2\gamma}$	4.24 ± 0.74	4.19 ± 0.73	3.63 ± 0.74	3.43 ± 0.78
CL = 10%, No. $2_{\eta\to 3\pi^0}$, No. $2_{2\pi^0,\eta\to 2\gamma}$	4.52 ± 0.68	4.34 ± 0.66	3.89 ± 0.67	3.79 ± 0.61
CL = 10%, No. $2_{\eta\to 3\pi^0}$, No. $3_{2\pi^0,\eta\to 2\gamma}$	4.00 ± 0.67	3.82 ± 0.65	3.53 ± 0.63	3.39 ± 0.64

values expected from our $\eta \to 2\gamma$ and $\eta \to 6\gamma$ events. Since our ratio BR($\eta \to 3\pi^0$)/BR($\eta \to \gamma\gamma$) = 0.795 is different from the PDG ratio by just 3.7%, the systematic uncertainty in the $\eta \to \pi^0\gamma\gamma$ signal due to this fixing is at the level of 0.02 times the $\eta \to 3\pi^0$-background/$\eta \to \pi^0\gamma\gamma$-signal ratio. For instance, if in the region of the η-meson mass, the $\eta \to 3\pi^0$-background/$\eta \to \pi^0\gamma\gamma$-signal ratio was 10, the corresponding systematic uncertainty would be about 20%. So by applying a cut on the effective radius of clusters, we decrease significantly the systematic uncertainty due to the $\eta \to 3\pi^0$ background.

The weight factor of the $\pi^- p \to \pi^0\pi^0 n$ background was a free parameter in the binned maximum-likelihood fits. Since the origin of this background is mostly the tails of the experimental resolutions of the two-photon invariant mass, there is some uncertainty in the quantitative reproduction of the $\pi^- p \to \pi^0\pi^0 n$ background fraction by the MC simulation.

The results for BR($\eta \to \pi^0\gamma\gamma$) obtained from the binned maximum-likelihood fits of the $m(\pi^0\gamma\gamma)$ spectra are given in Table II for different selection criteria: the vertex z-coordinate limits, the kinematic-fit confidence level, the $\eta \to 3\pi^0$ background (or parameter ρ) cut, and the $\pi^0\pi^0/\eta \to 2\gamma$ background [or $m_{\max}(\pi^0\gamma)$] cut. The errors in BR($\eta \to \pi^0\gamma\gamma$) are obtained by the MINOS procedure of the MINUIT package [24] for its "UP" parameter equal to the value reflecting one standard deviation for a fit with two free parameters. In our fits, these two free parameters were the $\eta \to \pi^0\gamma\gamma$ signal and the $\pi^- p \to \pi^0\pi^0 n$ background contributions.

The cases marked by a star in Table II are illustrated in Figs. 10–13. These figures show the experimental and MC-simulation spectra of the $m(\pi^0\gamma\gamma)$ invariant mass for events selected as the $\pi^- p \to \pi^0\gamma\gamma n$ candidates. The experimental LH_2 spectrum is shown before and after each background subtraction. Figure 10 illustrates the fitting procedure for

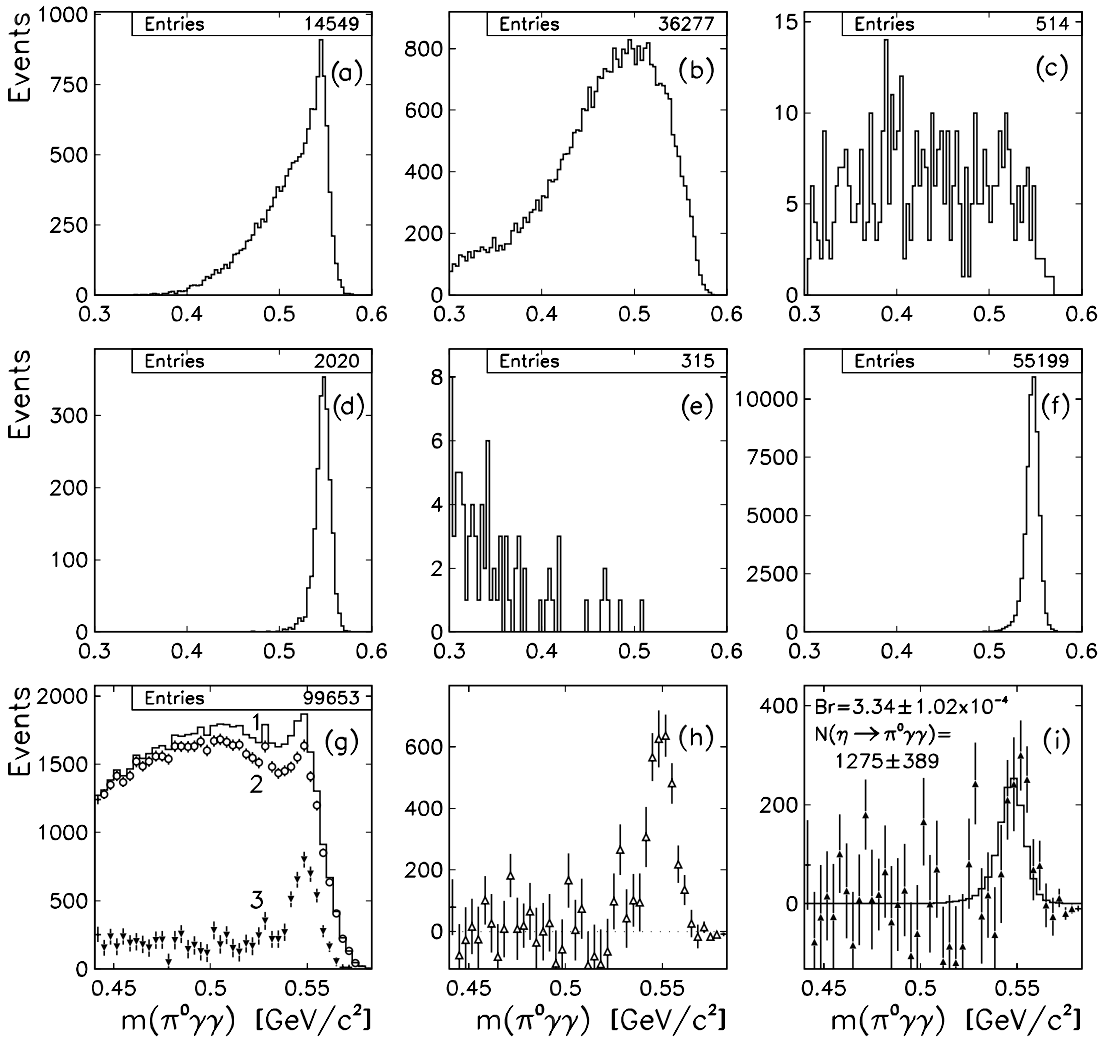

FIG. 11. Same as Fig. 10 except that a 20% CL is applied in the kinematic fit.

events selected at the 2% CL, with the vertex z coordinate within ± 6 cm, and after applying cut No. 2 on parameter ρ. As seen in Fig. 10, the $\eta \to 3\pi^0$ background subtracted in the η-mass region has the same magnitude as the $\eta \to \pi^0\gamma\gamma$ signal (which is 1683 ± 379 events), while the $\eta \to \gamma\gamma$ background subtracted is more than twice as large as the $\eta \to \pi^0\gamma\gamma$ signal. Figure 11 illustrates the fitting procedure for the samples that differ from the ones shown in Fig. 10 by tightening the kinematic-fit confidence level to 20%. As can be seen, this cut suppresses all background processes more than the signal, and leaves the $\eta \to \pi^0\gamma\gamma$ branching ratio at the same level. Figure 12 illustrates the fitting procedure for the samples that differ from the ones shown in Fig. 11 by applying the $m_{\max}(\pi^0\gamma)$ cut No. 1. As seen in Fig. 12, this cut suppresses almost all $\eta \to \gamma\gamma$ and much of the $\pi^- p \to \pi^0\pi^0 n$ background. The $\eta \to \pi^0\gamma\gamma$ branching ratio is still about the same. Figure 13 illustrates the fitting procedure for the samples that differ from the ones shown in Fig. 12 by applying the $m_{\max}(\pi^0\gamma)$ cut No. 2; i.e., further tightening the cut on the $\eta \to \gamma\gamma$ and the $\pi^- p \to \pi^0\pi^0 n$ background. As can be seen, the $\eta \to \pi^0\gamma\gamma$ branching ratio still does not change much.

The systematic uncertainties arising from applying different selection criteria are evaluated from the results given for $\mathrm{BR}(\eta \to \pi^0\gamma\gamma)$ in Table II. There is a small dependence on the vertex z coordinate; the branching ratio increases for a looser cut on the vertex z coordinate limits. We see two possible reasons that might cause this: (i) the very limited statistics for the empty-target sample, and (ii) some imperfections in reproducing the vertex z-coordinate distributions by the kinematic fit for events of the MC simulation for the background processes. Note that the vertex z coordinate from the kinematic fit of the background processes has little in common with the real vertex z coordinate of the background events themselves. Tightening only the cut on the kinematic-fit confidence level has little effect on the results. However, applying cuts on both parameter ρ and $m_{\max}(\pi^0\gamma)$ leads to slightly smaller values of $\mathrm{BR}(\eta \to \pi^0\gamma\gamma)$ for a tighter cut on the kinematic-fit confidence level. No systematic changes are seen when we apply different ρ cuts. There is some decrease in

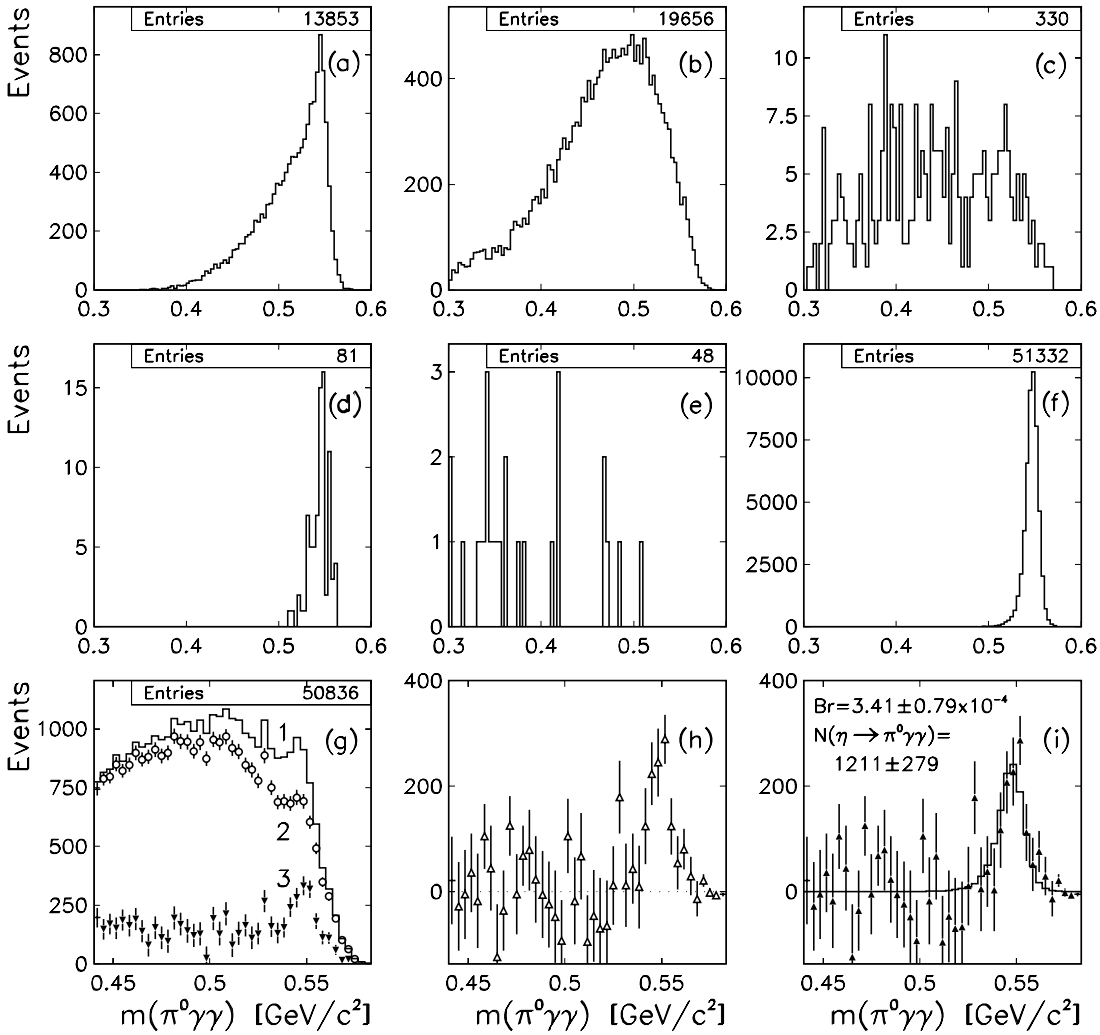

FIG. 12. Same as Fig. 11 except that cut No. 1 on $m_{\max}(\pi^0\gamma)$ has been applied.

branching-ratio values after tightening the cut on $m_{\max}(\pi^0\gamma)$. This could be due to some imperfections in reproducing the $\eta \to \gamma\gamma$ background in the MC simulation or to a difference of the $\eta \to \pi^0\gamma\gamma$ decay matrix element from the phase-space distribution used for this process in the MC simulation.

The reliable determination of the $\eta \to \pi^0\gamma\gamma$ decay matrix element from the present data is complicated. There are still some imperfections in the $\pi^- p \to \pi^0\pi^0 n$ background simulation and its combination with the CB resolutions. A future measurement of the $\eta \to \pi^0\gamma\gamma$ branching ratio and the decay matrix element will need a better beam momentum and energy resolution, and a sufficient set of empty-target data. Measuring the neutron kinematical quantities will also significantly improve the experimental resolution and decrease the background contamination.

The present analysis does not show a significant difference between the $m(\gamma\gamma)$ experimental spectrum for the $\eta \to \pi^0\gamma\gamma$ candidates and the spectrum obtained from the MC simulation for this reaction, in which this decay was generated according to phase space. However, there are large statistical uncertainties and possible systematics in the remaining spectrum due to subtraction of the background contributions. In Fig. 14, we illustrate the $m(\gamma\gamma)$ spectra (above the π^0-meson mass) obtained for events that satisfied the 2-C kinematic fit to hypothesis $\pi^- p \to \eta n \to \pi^0\gamma\gamma n$ at the 20% CL These events were preselected by testing the 1-C $\pi^- p \to \pi^0\gamma\gamma n$ hypothesis at the 20% CL, with the vertex z coordinate within ± 8 cm, after applying cut No. 2 on parameter ρ, and cut No. 2 on $m_{\max}(\pi^0\gamma)$. In Fig. 14(a), we show the spectrum that was obtained for all experimental candidates selected with the above criteria. The corresponding spectra for MC simulation of $\pi^- p \to \eta n \to 3\pi^0 n$, $\pi^- p \to \pi^0\pi^0 n$, and $\pi^- p \to \eta n \to \gamma\gamma n$ are shown in Figs. 14(b), 14(c) and 14(e). The empty-target spectrum is shown in Fig. 14(d). The experimental spectrum after subtraction of the $\eta \to 3\pi^0$ background subtraction only (open circles), and after subtraction of both the $\eta \to 3\pi^0$ and the $\pi^0\pi^0$ background contributions (solid triangles) is shown in Fig. 14(f). The $\eta \to \pi^0\gamma\gamma$ MC-simulation spectrum (shown by the solid line in the same figure) is normalized to the number of

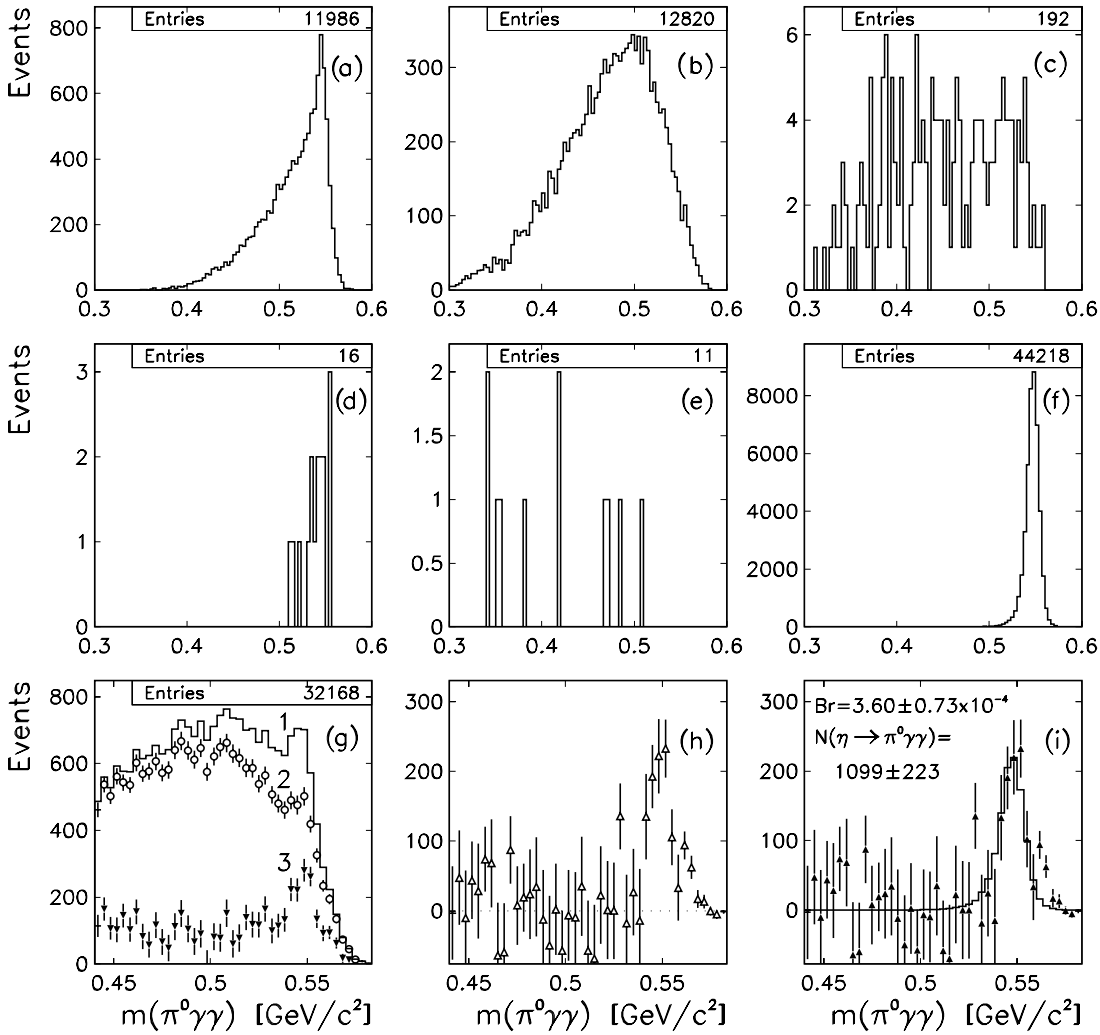

FIG. 13. Same as Fig. 11 except that cut No. 2 on $m_{\max}(\pi^0\gamma)$ has been applied.

$\eta \to \pi^0\gamma\gamma$ events obtained in the maximum-likelihood fit. The $\eta \to 3\pi^0$ background is subtracted according to its fixed weight factor. The subtraction of the $\pi^0\pi^0$ background is made according to the results of the same maximum-likelihood fit. The empty-target and the $\eta \to \gamma\gamma$ background contributions in the figure have not been subtracted. In Fig. 15, we show similar $m(\gamma\gamma)$ invariant-mass spectra that differ from the ones shown in Fig. 14 by further tightening the cut on $m_{\max}(\pi^0\gamma)$. The difference between the remaining experimental spectrum and the MC-simulation spectrum for $\eta \to \pi^0\gamma\gamma$ is of the same order of magnitude, as seen in Fig. 14(f).

To get our final result for the $\eta \to \pi^0\gamma\gamma$ branching ratio, we take an average of all results obtained when the vertex z-coordinate limits were ± 6 and ± 5 cm (i.e., with smaller uncertainties due to the subtraction of background contributions) and the ρ cuts were No. 2 and 3, which also result in significant decrease in the $\eta \to 3\pi^0$ background uncertainty. This gives

$$\mathrm{BR}(\eta \to \pi^0\gamma\gamma) = (3.5 \pm 0.7_{\mathrm{stat}} \pm 0.6_{\mathrm{syst}}) \times 10^{-4},$$

where the statistical uncertainty includes the effect of the fit errors. The systematic uncertainty includes all other major effects: (i) the variation in results due to different selection criteria; (ii) the uncertainty in the overall number of η mesons produced; (iii) the uncertainty due to fixing the weight fractions for the empty target and the $\eta \to 3\pi^0$ and $\eta \to \gamma\gamma$ backgrounds; (iv) the uncertainty due to the possible difference of the $\eta \to \pi^0\gamma\gamma$ decay matrix element from the phase-space distribution.

In order to compare our result with theoretical predictions, we must convert the branching ratio to the decay width. This needs the η-decay rate as input. For this purpose, we use $\Gamma(\eta \to \mathrm{all}) = 1.29 \pm 0.07$ keV from the latest edition of the Review of Particle Physics [21]. Then the decay width is

$$\Gamma(\eta \to \pi^0\gamma\gamma) = 0.45 \pm 0.09_{\mathrm{stat}} \pm 0.08_{\mathrm{syst}}\ \mathrm{eV}.$$

Adding the uncertainties in quadrature, we get $\Gamma(\eta \to \pi^0\gamma\gamma) = 0.45 \pm 0.12$ eV.

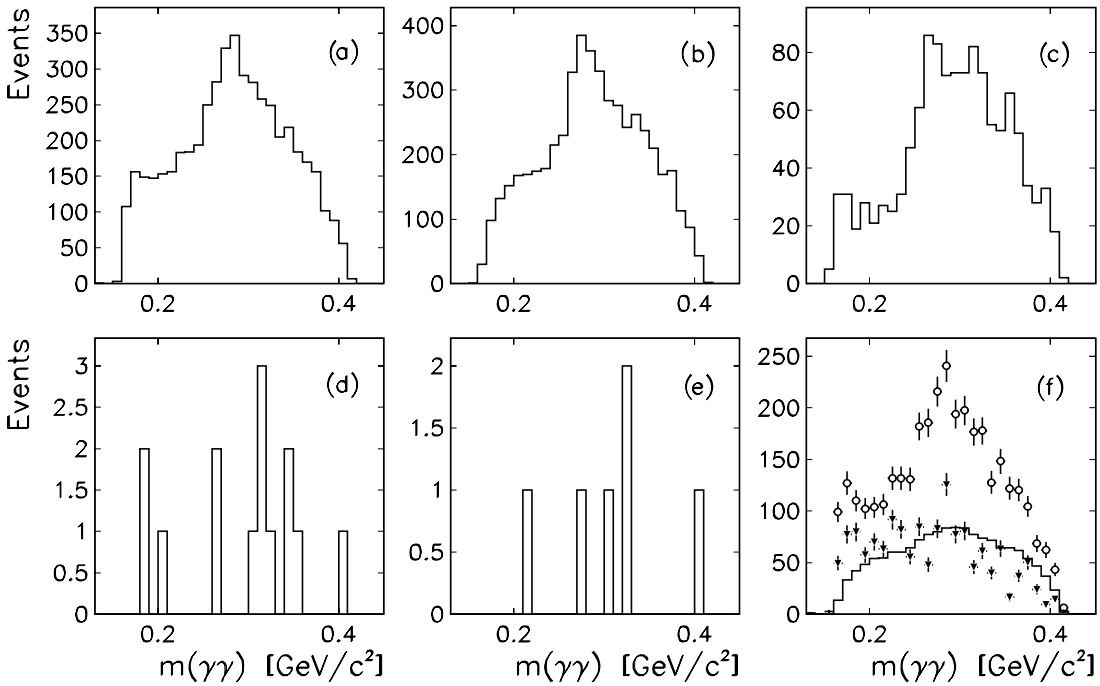

FIG. 14. The $m(\gamma\gamma)$ spectra (above the π^0-meson mass) obtained for events that satisfy the 2-C kinematic fit to the $\pi^- p \to \eta n \to \pi^0\gamma\gamma n$ hypothesis at the 20% CL. The events were preselected by testing the 1-C $\pi^- p \to \pi^0\gamma\gamma n$ hypothesis at the 20% CL, with the vertex z coordinate within ± 8 cm, after applying cut No. 2 on the parameter ρ, and cut No. 2 on $m_{\max}(\pi^0\gamma)$. (a) experimental LH_2 data, (b) MC simulation for 3×10^7 $\pi^- p \to \eta n \to 3\pi^0 n$ events, (c) MC for 4×10^7 $\pi^- p \to \pi^0\pi^0 n$ events, (d) empty-target data, (e) MC for 1×10^7 $\pi^- p \to \eta n \to \gamma\gamma n$ events, and (f) experimental LH_2 spectrum after subtraction of only the $\eta \to 3\pi^0$ background (open circles), and after subtraction of both the $\eta \to 3\pi^0$ and the $\pi^0\pi^0$ background contributions (solid triangles); the $\eta \to \pi^0\gamma\gamma$ MC-simulation spectrum (solid line) is normalized to the number of $\eta \to \pi^0\gamma\gamma$ events obtained by the maximum-likelihood fit. The $\eta \to 3\pi^0$ background is subtracted according to its fixed weight factor. The subtraction of the $\pi^0\pi^0$ background is made according to the results of the same maximum-likelihood fit. The empty-target and the $\eta \to \gamma\gamma$ background contributions are not subtracted in (f).

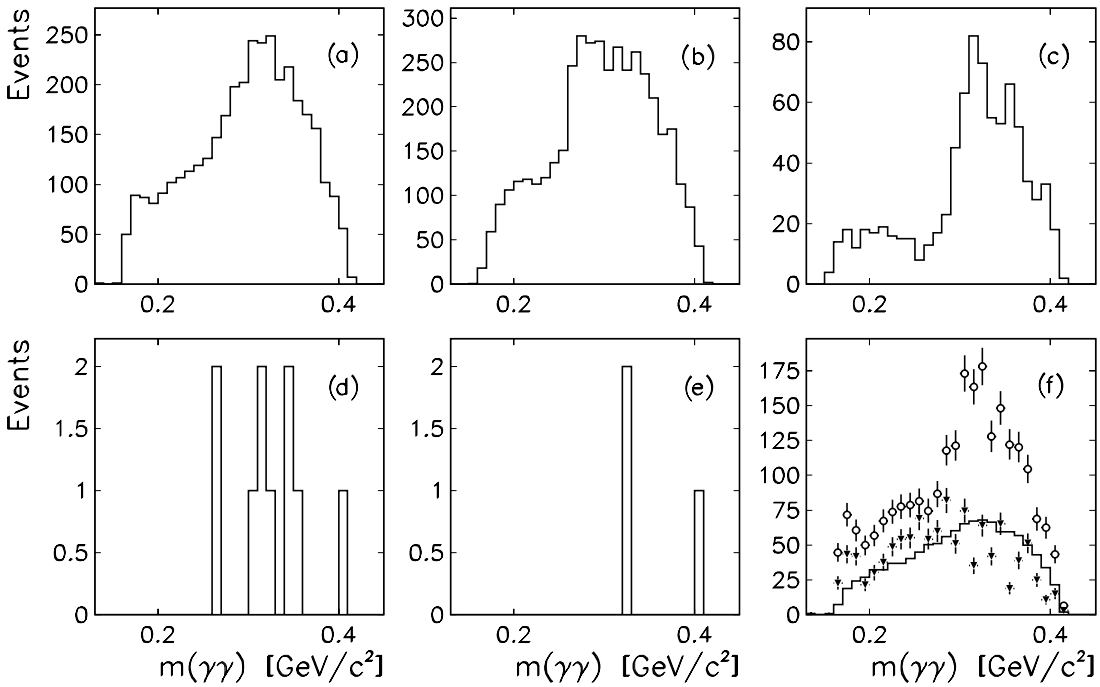

FIG. 15. Same as Fig. 14 except that cut No. 3 on $m_{\max}(\pi^0\gamma)$ has been applied.

VII. SUMMARY AND CONCLUSIONS

The final value of the branching ratio for the $\eta \to \pi^0\gamma\gamma$ rare decay measured with the Crystal Ball multiphoton spectrometer is $\mathrm{BR}(\eta \to \pi^0\gamma\gamma) = (3.5 \pm 0.7_{\mathrm{stat}} \pm 0.6_{\mathrm{syst}}) \times 10^{-4}$. This result is based on a signal of 1.6 thousand $\eta \to \pi^0\gamma\gamma$ decays extracted from 28 million η mesons produced at the BNL Alternating Gradient Synchrotron in the $\pi^- p \to \eta n$ reaction close to threshold. Our branching ratio is about one half the PDG value [21], which is based on the results of Ref. [12], and disagrees with it by about three standard deviations. At the same time, our result for $\mathrm{BR}(\eta \to \pi^0\gamma\gamma)$ is in good agreement with χPTh predictions. Our final result supersedes the preliminary result reported by us in Refs. [13,14]. The preliminary result did not include the empty-target subtraction and the correction for the $\eta \to \gamma\gamma$ background removal. Within errors, our result is also in agreement with the value obtained for $\Gamma(\eta \to \pi^0\gamma\gamma)$ in the independent analysis [15,16]; however, the number of the $\eta \to \pi^0\gamma\gamma$ experimental events extracted in our analysis is more than an order of magnitude larger.

ACKNOWLEDGMENTS

This work was supported in part by DOE and NSF, NSERC of Canada, the Russian Ministry of Industry, Science and Technologies, the Russian Foundation for Basic Research. We thank SLAC for the loan of the Crystal Ball. The assistance of BNL and AGS with the setup is much appreciated.

[1] J. Gasser and H. Leutwyler, Nucl. Phys. **B250**, 465 (1985).
[2] Ll. Ametller, J. Bijnens, A. Bramon, and F. Cornet, Phys. Lett. **B276**, 185 (1992).
[3] W. Alles, A. Baracca, and A. T. Ramos, Phys. Lett. **B349**, 555 (1995).
[4] P. Ko, Phys. Lett. **B349**, 555 (1995).
[5] S. Bellucci and C. Bruno, Nucl. Phys. **B452**, 626 (1995).
[6] J. Bijnens, A. Fayyazuddin, and J. Prades, Phys. Lett. **B379**, 209 (1996).
[7] J. N. Ng and D. J. Peters, Phys. Rev. D **46**, 5034 (1992).
[8] M. Jetter, Nucl. Phys. **B459**, 283 (1996).
[9] E. Oset, J. R. Peláez, and L. Roca, Phys. Rev. D **67**, 073013 (2003).
[10] M. M. Achasov *et al*. (SND Collaboration), Nucl. Phys. **B600**, 3 (2001).
[11] F. Binon *et al*., Yad. Fiz. **33**, 1534 (1982); Lett. Nuovo Cimento A **71**, 497 (1982).
[12] D. Alde *et al*. (GAMS-2000 Collaboration), Yad. Fiz. **40**, 1447 (1984); Z. Phys. C **25**, 225 (1984).
[13] S. Prakhov (Crystal Ball Collaboration), Phys. At. Nucl. **65**, 2238 (2002).
[14] B. M. K. Nefkens and J. W. Price, *Eta Physics Handbook*, Phys. Scr. T **99**, 114 (2002).
[15] N. S. Knecht, Ph.D. Thesis, University of Regina, 2002.
[16] N. Knecht *et al*., Phys. Lett. **B589**, 14 (2004).
[17] S. Prakhov *et al*. (Crystal Ball Collaboration), Phys. Rev. C **69**, 045202 (2004).
[18] W. B. Tippens *et al*. (Crystal Ball Collaboration), Phys. Rev. Lett. **87**, 192001 (2001).
[19] A. Starostin *et al*. (Crystal Ball Collaboration), Phys. Rev. C **64**, 055205 (2001).
[20] A. Starostin *et al*. (Crystal Ball Collaboration), Phys. Rev. C **67**, 068201 (2003).
[21] S. Eidelman *et al*. (Particle Data Group), Phys. Lett. **B592**, 1 (2004).
[22] HBOOK—Statistical Analysis and Histogramming, CERN Program Library.
[23] S. Prakhov, CB report CB-04-002 (web page—http://bmkn8.physics.ucla.edu/Crystalball/-Docs/-documentation.html).
[24] MINUIT—Function Minimization and Error Analysis, CERN Program Library.